

Adhesion testing of coated surfaces

Programme of Scientific Support
To Standardisation

Stage II

Final report



PRIME MINISTER'S
SERVICES
SCIENTIFIC,
TECHNICAL AND
CULTURAL AFFAIRS

Table of contents

0	SUMMARY	4
1	INTRODUCTION	10
1.1	Context of the research programme	10
1.2	Objectives	10
1.3	Outline	11
2	METHODOLOGY	12
2.1	Selected coatings (WP1)	12
2.1.1	Substrates	12
2.1.2	Coatings	12
2.2	Characterisation: Experimental Set-up	14
2.2.1	Crater grinding (coating thickness)	15
2.2.2	Laser profilometer (surface roughness)	15
2.2.3	Contact profilometer (surface roughness)	16
2.2.4	Macro-indentation (composite hardness)	16
2.2.5	Depth sensing indentation (coating hardness and Young's modulus)	17
2.2.6	Electron probe microanalysis (composition)	17
2.2.7	Auger spectroscopy (composition)	18
2.2.8	Bending beam stress measurements	18
2.2.9	XRD Stress measurements	19
2.2.10	Raman spectroscopy (DLC structure)	19
2.3	Theoretical principles of adhesion tests	20
2.3.1	Scratch Adhesion Test	20
2.3.2	Rockwell Indentation Adhesion Test	21
2.3.3	Four Point Bending Adhesion Test	22
2.3.4	Tensile Adhesion Test	23
2.3.4.1	principle	23
2.3.4.2	Models	25
2.3.4.3	Crack density distribution	26
2.3.4.4	Film Decohesion	27
2.3.4.5	Applicability	29
2.4	Adhesion Testing: Experimental Set-Up	30
2.4.1	Scratch test	30
2.4.2	Indentation test	30
2.4.3	Four-point bending	31
2.4.4	Tensile testing	31

3	RESULTS	32
3.1	Deposition of the Coatings: WP1	32
3.1.1	PACVD DLC (Vito)	32
3.1.2	CVD TiN (WTCM)	33
3.1.3	Electrodeposited Zn (ULB)	34
3.2	Characterisation: WP2	36
3.2.1	Introduction	36
3.2.2	Coating thickness	36
3.2.3	Surface roughness	37
3.2.4	Composite hardness	39
3.2.5	Coating hardness and Young's modulus	39
3.2.6	Composition	41
3.2.7	Coating microstructure and morphology	41
3.2.8	Internal stress	42
3.2.8.1	Bending beam stress measurements on DLC	42
3.2.8.2	Bending beam and XRD stress measurements on TiN	42
3.2.8.3	XRD stress measurements on Zn	44
3.2.9	Preferential orientation	44
3.2.10	DLC structure	44
3.2.11	scratch test	45
3.3	Adhesion Tests: WP3	46
3.3.1	scratch tests	46
3.3.1.1	Single Pass Scratch Test	46
3.3.1.2	Constant Load Scratch Test	50
3.3.1.3	Multipass Scratch Test	51
3.3.1.4	Overview	52
3.3.1.5	Damage at scratch styli	52
3.3.1.6	Conclusion	53
3.3.2	Indentation	54
3.3.2.1	results	54
3.3.2.2	Conclusion	55
3.3.3	Four point bending adhesion test	56
3.3.3.1	results	56
3.3.3.2	conclusion	58
3.3.4	Tensile Adhesion Testing	59
3.3.4.1	DLC-coatings	59
3.3.4.2	TiN coatings	62
3.3.4.3	Conclusion	62
3.4	Overview of the Results	63
4	CONCLUSIONS	64
4.1	General Conclusions	64
4.2	Future research issues	64

0 SUMMARY

Surface engineering is a generic technology and is used in a wide range of applications in all industrial sectors including the aerospace, automotive, engineering, construction, biomedical, textile, optical and microelectronics industries. Advanced surface coatings add physical properties, such as lubricity, hardness, or corrosion resistance, to lower-valued substrates that improve the overall quality of the component. In many cases there is a synergetic combination of the properties of the bulk material and the coating. For example, hard coatings on tough substrates are less vulnerable to catastrophic failures than hard bulk materials.

Coating technology is fundamentally dependent upon good adhesion between the coating and the substrate, and in many cases adhesion is the limiting factor for the wider application of the technology. The OSTC project Adhesion testing of Coated Surfaces addresses at this key aspect of coatings. Various engineering methods are used to measure the adhesion. Other methods which are able to quantify the adhesion more directly are being developed. An urgent need to make adhesion values interchangeable between companies is felt. The first step towards this objective is a thorough understanding of the test methods and a clear definition of their validity and limitations. The second step is the standardisation of the tests, which makes an objective and universally accepted quality assurance of the adhesion of coatings possible.

Four adhesion test methods were examined in this project. The scratch test is an engineering adhesion test method which consists of drawing a diamond stylus across the surface under increasing normal load, either stepwise or continuously, until coating spallation failure events are observed in the scratch track. The normal load at which this failure occurs is called the critical normal load L_c (unit: N). This *scratch adhesion test* can be operated in 3 different modes. The first mode is the conventional way of applying the scratch test, i.e. an increasing load with specified ramp is applied on the scratch stylus while the specimen is moved underneath it. This is the "*single pass scratch test (SPST)*". The position along the scratch track where this failure event is produced is evaluated by optical microscopy, and the corresponding normal load can easily be calculated from the test conditions. This load L_c is related to the adhesion of the coating. In the second mode, i.e. the "*constant load scratch test (CLST)*", separate scratches are made at a constant load, and the load is increased between successive scratches. Again, the load provoking failure is defined as the critical load L_c . In the "*multipass scratch test (MPST)*" mode the specimen is subjected to repeated scratching under a constant sub-critical load within the same scratch track. The number of passes at which the first failure event appears is then the criterion for adhesion.

The second adhesion test method is the *Rockwell indentation test*. This method has an even more simple concept than the scratch tests and can be performed with a Rockwell hardness tester. An indent is made in the material and the nature of the damage of the coating nearby the indent is evaluated microscopically using predefined failure classes.

A more direct measurement of the adhesion is offered by the *four point bending adhesion test*. A crack is initiated between the coating and the substrate, e.g. by chemical dissolution of the interface. A shear stress is now imposed at the interface by a four point bending test. At the moment the crack is propagating, the total energy to sustain the shear starts to decrease. This energy release is a direct measure of the adhesion.

The last adhesion test method makes use of a tensile test, i.e the *tensile crack spacing test*. The coated sample is subjected to an increasing tensile strain, causing the film to crack and break into segments. The maximal shear stress at the interface, which is assumed to be related with the adhesion of the coating, can be calculated from the film tensile strength, the coating thickness and the crack spacing distribution. If the crack spacing distribution is scattered, the average value of the spacing is more appropriate. Situations where delamination at the interface occurs can also be taken into account. In the latter case, the energy release rate for film decohesion may be evaluated. It is evident that the coating has to be significantly more fragile than the substrate in order to induce cracking in the coating.

These four adhesion test methods were explored in this project. Parameters of the test set-ups were changed to evaluate the sensitivity of the method to these test parameters. In addition, different coating-substrate systems with different properties were used. This work has led to the evaluation of the applicability of the different test methods and the reliability of the results.

The **selected coatings** were PACVD DLC on C60 steel, PVD TiN on ASP23 steel and electrodeposited Zn on automotive steel. Two different types of each coating were produced with the aim of varying the adhesion, and a third coating with different properties but good adhesion to study the effect of coating intrinsic properties on the result. The *DLC coatings* are known for their good sliding wear resistance. The adhesion on the steel substrate is assured by an $a\text{-Si}_{1-x}\text{C}_x\text{:H}$ interlayer. The carbon content in that interlayer is a parameter governing the adhesion. A poorer adhering coating has been deposited by increasing the C content in the interlayer. A third variant of the DLC coatings was produced at a lower bias voltage, yielding a more polymer-like (soft) top coating.

TiN coatings are hard and brittle, frequently used in machining tools to enhance the life cycle. They are deposited at 450°C. A Ti interlayer is needed for the adhesion of the coating on the steel. The bias voltage during the deposition of that interlayer was changed for making a less adhering coating. A third variant of the coating was deposited at a lower temperature (200°C).

The *electrodeposited Zn coating* is mainly used for corrosion protection of steel products. A badly adherent coating was produced by first growing an oxide layer on the steel substrate in a FeCl_3 solution. A third variant was deposited at a higher current density in the electrolytic cell, namely 100 A/dm² instead of the normally used 75 A/dm² for this kind of coating.

A thorough **characterisation** of the obtained coatings was necessary in order to get a better understanding of the results of the different adhesion test methods.

The *thickness* of the coatings was measured by the crater grinding or Calo test. Typical values for the DLC coatings are between 1.5 and 2.5 µm, for the TiN coatings between 2.5 and 4 µm and for the Zn coatings between 40 and 50 µm.

The *surface roughness* of the coated samples was examined by contact profilometry. The measurements were repeated by the three research partners and can be considered as a limited round robin test. When the same tip radius was used (5 µm), the results were within the margin of error. One partner used a larger tip (radius 12.5 µm) which logically resulted in systematically lower surface roughness values.

The *hardness of the coating* and its elastic modulus were measured by nanoindentation. This is a hardness indentation technique which is restricted to the first few hundred nanometers of the material surface to avoid the influence of the substrate. The load and displacement are recorded during the measurement. The results of the nanoindentation confirmed that the TiN are hard and stiff coatings. The obtained values on the DLC coatings gave an expected, but remarkable insight in the differences between the variants. The polymer-like type has only one fourth of the hardness of the other variants. The Zn coatings are soft and showed creep during the indentation test.

The *internal stress state* of the coatings was examined by three different methods. Two of them are based on X-ray diffraction, namely the classical $d\text{-sin}^2\psi$ technique and the novel LIBAD (low incident beam angle technique) which is developed especially for thin coatings. The third technique is the bending beam stress measurement, a mechanical method in which the deflection of a glass strip is measured after coating it. The three techniques were used on the TiN coatings. The resemblance of the results by the different methods was good, on the condition that the elastic modulus measured by the nanoindentation was used. The intrinsic stress in the TiN coatings peaks at nearly -5 GPa compressive stress. The internal stress in the DLC could only be measured by the mechanical method since the coating is amorphous and does not produce X-ray diffraction peaks. The stress is also compressive and amounts to -2 GPa. The internal stress in the polymer-like variant is half as high. Finally, the internal stress in the Zn coating was only measured with the $d\text{-sin}^2\psi$ method. Here, the stress is rather low and only a few tens of MPa is reached. If higher stresses were build up during the deposition, they are levelled out by creep in the coating.

Further characterisation of the coatings has been done on the *composition* by EPMA and AES, and on the *morphology* by SEM and OM. The conclusions drawn from these investigations are mainly confirming the differences in interface layer for the poor adherent DLC and TiN coating. It also results from Raman measurements that the third variant of the DLC coatings is indeed polymer like.

The characterisation of the used coatings has created a solid base for the evaluation and understanding of the results obtained by the different adhesion test methods. Hereafter, these adhesion tests and their particularities are discussed one by one.

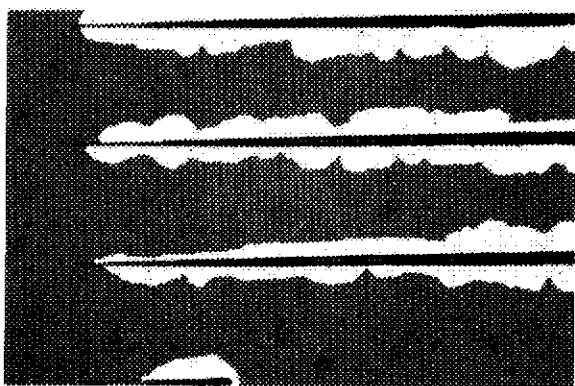


Fig. 1 Flaking of a (intentionally made) poor adherent DLC coating along a scratch track.

The **single pass scratch test** is used classically as an engineering method to assess the adhesion. The test results clearly learn us that the critical load L_c may not be considered as stand-alone criterion of the adhesion. Although the good and poor adhering DLC coating show the same L_c , the failure at L_c is of a completely different nature: the good adherent variant exhibits spallation within the scratch track, while gross flaking in and around the scratch track is produced in the other specimen (fig. 1), which clearly demonstrates the poorer

adhesion of the latter. The modified DLC coating (the polymer-like) has a considerably higher L_c . This correlates with its lower internal stress and hardness value.

For the TiN variants as well, no significant difference in critical load value for the good and poor adherent variants could be measured using the single pass progressive load mode scratch test. Moreover, the failure mode and magnitude of the failure events are virtually the same. Both TiN variants spall at the border of the scratch track, exposing the substrate surface. The third variant showed a quite different 'buckling type' failure event and hence, its critical load value cannot be directly compared to those of the other variants.

When using the scratch test on the Zn coating, a perforation of the coating was obtained without any failure mode related to the adhesion. The stylus is ploughing through the coating material. The scratch test method thus can not be used to characterise the adhesion properties of conventional ductile electro-deposited Zn coatings.

The **CLST mode** scratch test enabled to better discriminate between the good and poor adherent DLC and TiN coatings. Higher values of L_c were found for the good adherent DLC coating than obtained by the SPST. It was proven by acoustic emission and frictional force measurements that failure starts in the progressive load mode at a higher load (further away of the beginning of the track) than observed afterwards by optical microscopy. This indicates that the increasing load can induce spallation of delaminated parts of the coating behind the scratch stylus. In other words, a spallation event may be running backwards in the direction of the start of the scratch track at a certain load. We can conclude that the CLST method is more reliable and more sensitive to discriminate coatings on the basis of adhesion. Unfortunately, this method is also more time consuming.

The **multipass scratch test** is even more time- and effort consuming. More information is gained by this test about the toughness and fatigue resistance of the coatings. Due to the excellent toughness properties of the DLC coatings, no coating failure was induced in this mode at a slightly lower load than the L_c obtained by the CLST. The brittle TiN on the other hand showed progressive damaging during the MPST. It was possible to discriminate between the good and poor adherent TiN coatings based by the number of passes before regular spallation failure is observed.

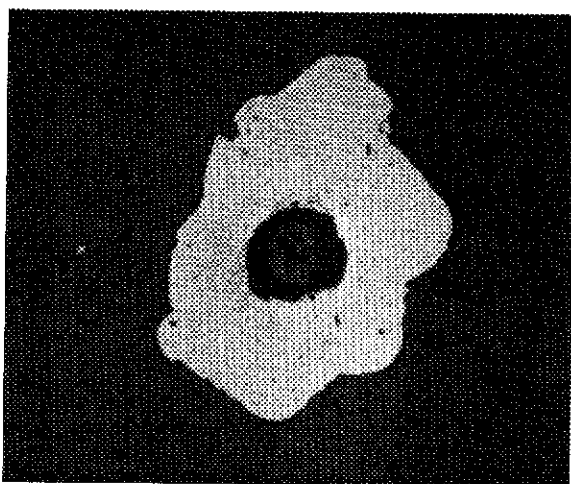


Fig. 2 Indentation adhesion test on a bad adherent DLC coating. A spallation occurred around the indent.

The results of the **indentation adhesion test** are in general parallel to those of the scratch test. The test parameters under investigation were the indentation speed, the hold time after indentation and the indentation load. No significant influence on the results by varying the two first parameters could be found. The failure event became more pronounced with increasing load. On the other hand, there was no transition from one failure mode to another while changing the load. TiN coatings crack at the edge of the indents, while all DLC coatings flake off upon indentation. Discrimination of the good and poor adherent DLC coatings was only possible when the extent of the

spallation, and not only the failure mode in itself, is considered. No spallation nor cracking could be provoked in the soft and ductile Zn coatings, hence this method can not be used to assess the adhesion properties of soft coatings. In general, we can conclude that less information is obtained by the indentation adhesion test than by the scratch test although subsequent indents at increasing normal loads would be a valuable alternative for the latter.

For DLC and Zn coatings the **four point bending technique** is implemented with success. The method gives a direct measure of the strength of the coating-substrate interface. However, the method is complicated and requires careful sample preparation. The test is only applicable if a precrack at the interface can be generated in situ. For the DLC an appropriate method based on the selective dissolution of the interface in a concentrated KOH solution was found. However, it was impossible to initiate crack propagation at the TiN-substrate interface, hence the method could not be applied on the TiN coatings. The numerical test results of the Zn and DLC coatings were as expected, except for the polymer-like DLC in which a different failure mechanism governed the crack propagation.

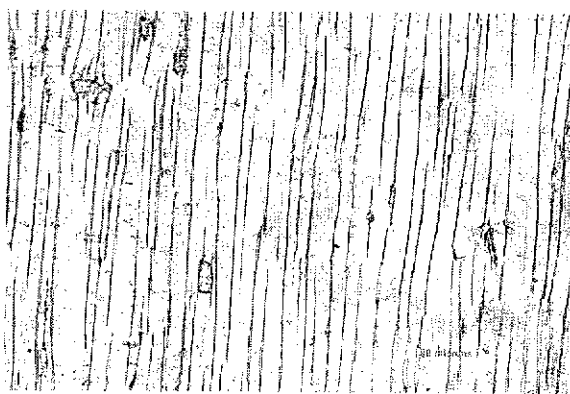


Fig. 3 Picture of the crack spacing at saturation for the good adherent DLC coating on automotive steel (taken by optical microscopy).

The last examined adhesion test method is the **tensile crack spacing technique**. The method showed its applicability for brittle coatings on ductile substrates. Qualitatively, the results for the TiN and DLC coatings (see fig. 3) were as expected, except for the poor adherent DLC coating where spallation occurred. The test can not be used for the ductile Zn coatings.

Different models exist to obtain the maximum interfacial shear strength from the film thickness. Their implementation does not change the qualitative ranking of the coatings, but the absolute values can

differ by a factor 3. However, numerous remarks can be made on the relative values of τ_1 obtained in the tensile adhesion test. Delamination of the coating is not always obvious when it occurs during the test, unless the coating really flakes off from the substrate. Scanning acoustic microscopy could be used to verify eventual delamination. If the measured (macro-)stress in the DLC coatings is taken into account, the absolute value of the good adherent DLC variants are closer to each other. In the case of TiN, the internal stress (IS) measured by XRD is taken into account. However, the situation here is much more complicated. Internal stresses measured by XRD correspond to the local stress, i.e. the sum of the macrostress and micro- or intrinsic stress is obtained. Only the macrostress is relaxed upon cracking of the coating. In this work, no distinction was made between micro- and macrostress.

The numerical results of the different adhesion test are summarised in the following table:

Technique	Scratch Test SPST	Scratch Test CLST	Scratch Test MPST	Indentation Test	Crack Propagation Test	Crack Spacing Test
coating	L_c [N]	L_c [N]	number of passes	class	G_c [J/m ²]	τ_f [Gpa]
DLC A	7.6	12	-	6	523	1.33
DLC B	8.6	8	-	6	24	(1.35)
DLC C	19.8	15	-	no failure	112	0.84
TiN A	78.8	80	15 passes	1	-	2.23
TiN B	74.4	60	10 passes	1	-	2.46
TiN C	76.4	64	15 passes	1	-	0.86
Zn A	-	-	-	-	233	-
Zn B	-	-	-	-	82	-
Zn C	-	-	-	-	168	-

The knowledge and better understanding gained by this work of different adhesion tests has led to the redaction of an improved pre-Standard ENV 1071-3 on the scratch test, the preparation of a pre-standard (ENV) concerning the Rockwell C indentation adhesion test and the draft guidelines for the four point bending crack propagation method on one hand and on the crack spacing method on the other.

1 INTRODUCTION

1.1 Context of the research programme

Deposition of coatings as surface improvement is a well-established technology and is an extremely versatile means of adapting component performance to severe working conditions. It is used in a wide range of applications in all industrial sectors including the aerospace, automotive, engineering, construction, biomedical, optical and microelectronics industries.

An **urgent need for standardisation** in this important area is felt. Indeed, the relatively slow uptake of coating technology stems largely from a lack of end-user confidence in the quality of coatings supplied to them. This project deals with one important aspect of coatings that is essential to guarantee their properties, functional characteristics and performance, namely the **adhesion** between the coating and the substrate.

At present, adhesion of coatings is routinely tested in industry by two **engineering adhesion tests**: the scratch test and the Rockwell indentation test. These engineering adhesion test methods, **however, yield 'adhesion values' which depend not only on basic adhesion, i.e. the interfacial bond strength, but also on other factors**, which are related both to the test itself (scratching velocity, stylus geometry, etc.) and to other coating/substrate composite properties (hardness, roughness, coating thickness, etc.). Furthermore, only some of the observed failure events are related to detachment at the coating/substrate interface and are thus relevant as a measure of adhesion. Other failure events, such as **cohesive failure** within the coating or substrate may occur but clearly cannot be used to assess the coating/substrate adhesive strength.

Various attempts have been made to obtain a **direct quantitative measure of adhesion** which include, for example, laser pulse and ultra-centrifuge techniques, but these are either difficult to use or not completely devoid of ambiguity. Some work has already been carried out to develop a relatively simple and unambiguous quantitative adhesion test based on tensile testing which has given encouraging results.

1.2 Objectives

The main **objective** of this project was to obtain an increased understanding in the validity of the conventional engineering test methods for measuring adhesion. Therefore, results from the engineering methods are compared with results obtained by the novel quantitative tensile adhesion test. To this end, series of industrially relevant coatings with different properties have been produced with various levels of adhesion, by deliberately varying the substrate cleaning procedures and/or adhesion interlayer structure.

This study **results** in:

- 1) A better understanding of scratch test results, and resulting a revision of the ENV 1071-3:1994 'Determination of Adhesion by a Scratch Test'.
- 2) Increased knowledge concerning the Rockwell indentation method. A draft standard for an ENV is produced and submitted to CEN TC184/WG5.

3) Improved practical experience with the four point bending adhesion test and the tensile adhesion test. Guidelines for testing are prepared and submitted to CEN TC184/WG5 for consideration to adopt as an ENV.

1.3 Outline

This reports is divided in two main parts. The first part describes the methodology used in the set up of the tests. The selection of different types of coatings is presented and justified in the view of the adhesion tests. Thereafter, the various characterisation techniques for the coatings are enumerated and their principle and experimental set-up are briefly exposed. Finally, the theoretical principles of the four adhesion test under investigation and the used experimental set-ups are discussed in detail.

The second part of the report gives the results of the research program. According to the work program, the results of the deposition of the coatings (WP1), of the coating characterisation (WP2) and of the adhesion tests (WP3) are presented respectively.

The report is completed by the general conclusions and by some recommendations for future R&D.

The revised standard ENV 1071-3:1994 'Determination of Adhesion by a Scratch Test', the improved draft standard on indentation adhesion testing and the guidelines of test for the tensile test methods will be described in individual reports to be supplied by Vito, WTCM and ULB respectively.

2 METHODOLOGY

2.1 Selected coatings (WP1)

2.1.1 Substrates

Different types of substrates have been used depending on the coating to be deposited on it and the envisaged adhesion test.

For task WP1.2 (deposition of TiN) a ASP23 (1.3343) has been chosen.

The DLC coatings were deposited (task WP1.3) on DIN C60 as substrate material.

The electrodeposited Zn coatings (task 1.1) layed on a automotive steel.

In a later stadium of the project, the need was risen for some TiN and DLC coatings on automotive steel as well, to make the tensile adhesion test possible. More details on these exceptions are given in §3.1.1 and 3.1.2.

The dimension of the substrates was 30x30x5 mm³ for the scratch test and the Rockwell indentation test and 120x20x15 mm³ for the four-point bending test.

The substrates were numbered at one side, hardened, and polished at the other side (1 µm diamond finish).

2.1.2 Coatings

3 different types of coatings have been produced and tested:

- plasma assisted chemical vapour deposited diamond like carbon (PACVD DLC, Vito)
- physical vapour deposited titanium-nitride (PVD TiN, WTCM)
- electrodeposited zinc alloys (Zn, ULB)

These coatings have been chosen because of their industrial relevance and distinct mechanical properties. Typical literature hardness (H) and Young's modulus (E) values are: Zn (H = 0.7 GPa, E = 105 GPa), TiN (H = 25 GPa, E = 350 GPa) and DLC (H = 20 GPa, E = 150 GPa).

Three variants were produced by varying the deposition parameters for each coating material:

- variant A: standard coating with good adhesion.
- variant B: standard coating with poor adhesion.
- variant C: modified coating with good adhesion.

PACVD DLC (Vito – WP1.3)

This coating material combines high wear resistance with low friction, making it ideally suited for sliding wear applications such as bearings, gears and machine parts in general. The lifetime of the wear part is prolonged while at the same time the energy consumption of the machine is reduced. The industrial relevance of this material is generally acknowledged and it is expected that the market for DLC and related coatings will grow rapidly.

DLC coatings are produced by a capacitively coupled r.f. (13.56 MHz) PACVD process from CH₄ - H₂ precursors. The substrates are placed on the powered electrode which is subjected to an ion bombardment due to the negative self-bias, which develops as a

consequence of the difference in mobility between ions and electrons. The biasing conditions are controlled to produce coatings with optimum mechanical properties. The adhesion between the coating and the substrate is deliberately varied by changing the structure of a Si containing interlayer which is necessary to let a DLC layer adhere to an iron alloy. The coating thickness typically varies between 1 and 3 μm .

PVD TiN (WTCM – WP1.2)

Titanium-nitride coatings have found wide practice in industry because of their high wear resistance and good corrosion properties. Typical applications are protective coatings for metal machining tools, gears and dies as well as for esthetical purposes because of its golden colour.

The coatings are deposited in a Balzers industrial-size, PVD triode ion-plating equipment. The substrates are rotated in front of a Ti sputtering target under a nitrogen containing atmosphere. A DC substrate bias of -150 V is applied to the substrates to obtain TiN coatings with optimum mechanical properties. A typical high speed steel, such as for example DIN S-6-5-2 (WN 1.3343) is normally used as substrate material and the adhesion between the coating and the substrate is deliberately varied by changing the structure of the Ti adhesion interlayer. The coating thickness typically varies between 2 and 5 μm .

ELECTRODEPOSITED ZINC (ULB – WP1.1)

Zinc coatings and zinc alloy coatings (ZnFe, ZnNi, ZnMn, ZnCo, ...) are commonly used in industry for protecting steel against corrosion. Especially due to the increased use in the automotive industry, the production of electrogalvanised steel has become an important product output for steel producers.

These Zn alloy coatings are increasingly being produced by high current density electroplating of steel coils. Processes used on a large industrial scale require close control of current density and hydrodynamic conditions at the surface of the continuous steel sheet. Current densities ranging from 90 to 150 A/dm^2 and Reynolds numbers between 15 000 and 60 000 are currently achieved. Electrolytes are acidic, chloride or sulphate, without organic additives. They may be either highly acidic ($\text{pH} < 1$, up to 130 g/l H_2SO_4) or slightly acidic ($\text{pH} \approx 3.5$). The thickness of the here deposited coatings vary typically between 10 and 20 μm . The adhesion between the coating and the substrate is deliberately varied by changing the electroplating parameters (the current density) and by modifying the steel surface preparation.

2.2 Characterisation: Experimental Set-up

Property	Technique	Partner
coating thickness	crater grinding	Vito
	cross section scanning electron microscopy	WTCM
surface roughness	laser profilometer	Vito
	contact profilometer	ULB, WTCM, Vito
composite hardness	macro-indentation	WTCM
coating hardness and Young's modulus	depth-sensing indentation	Vito
composition	electron probe microanalysis (EPMA)	Vito
	Auger spectroscopy (AES)	ULB
coating microstructure	cross section scanning electron microscopy	WTCM
residual strain preferential orientation	full X-ray diffraction (XRD) spectrum	ULB
DLC structure	Raman spectroscopy	Vito

We will shortly describe the principle and the experimental set-up of each of the characterisation techniques:

2.2.1 Crater grinding (coating thickness)

A spherical cap is ground into the coated specimen by rotating a ball, wetted by a suspension of diamond particles in ethanol, against that specimen. The test is stopped when the bottom of the crater has reached the substrate. The coating thickness t is calculated from the difference in diameter of the craters delimiting the outer coating surface and the interface between the coating and the substrate respectively.

This test is also called the Calo-test or the ball crater test.

Experimental (Vito):

A CSEM Calotest instrument was used to carry out the thickness measurements.

The ball, 30 mm in diameter, was made out of 100Cr6 bearing steel (ISO 3290), and the abrasive medium consisted of 1 μ m diamond paste suspended in ethanol, using a mixture of 1:4. The test is continued until the substrate is visible, and this typically takes a few minutes.

Five measurements per specimen were done.

2.2.2 Laser profilometer (surface roughness)

A light beam is focused on the surface. The roughness results in changes of the focus. There are advantages and limitations for each technique. The stylus may cause surface damage if the loading is too large. The lateral resolution is determined by the beam spot size, wavelength of light and by the resolution of the microscope lenses and other optical elements in the instrument.

Experimental (Vito):

An UBM ITF 100 A combined contact stylus - laser profilometer is used.

optical mode:

wavelength:	780 nm;
beam spot diameter:	1 μ m;
measurement range:	$\pm 50 \mu$ m or $\pm 500 \mu$ m;
resolution:	< 0.01 % of range.

In each measurement mode, six measurements per specimen were done (3 measurements in two orthogonal directions, parallel with the specimen edges)

2.2.3 Contact profilometer (surface roughness)

This technique measures surface profiles with a diamond stylus probe that touches the surface. The main disadvantage of this technique is that the stylus may cause surface damage if the loading is too large. The lateral resolution of surface features depends on both the stylus radius and the slopes of the surface features being profiled. Measured surface roughness parameters may strongly depend on the lateral resolution of the profilometer.

Experimental (Vito, WTCM, ULB):

Vito: see above (2.2.2).

An UBM ITF 100 combined contact stylus - laser profilometer
contact mode:

diamond stylus tip radius: 5 μm ;
stylus load: 0.7 mN;
measurement range: $\pm 100 \mu\text{m}$;
vertical resolution: 1 nm.

WTCM: Perthen S8P profilometer.

A skidless pick-up with a stylus tip radius of 5 μm was used. The tracing force was 0.9 mN (approx.).

ULB: Dektak 3030 profilometer.

Tracing force = 0.1 mN, stylus tip radius = 12.5 μm .

2.2.4 Macro-indentation (composite hardness)

Experimental (WTCM):

The composite hardness was measured by a Hoytom 1003A Rockwell tester.

For a Rockwell C measurement a sphero-conical diamond indenter is used with a 120° deg angle with a spherical apex of 0.200 mm. A minimum load of 10 kg and a maximum load of 150 kg are used.

For Rockwell A measurements the same indenter is used. The major load in this case however is 60 kg.

2.2.5 Depth sensing indentation (coating hardness and Young's modulus)

In the depth sensing indentation (DSI) (also called nano-indentation) technique, load and indenter displacement are recorded in situ to obtain an indentation hysteresis curve. Not only the hardness but also the elastic (Young's) modulus can be derived from this curve. The resolutions of the method, typically 10 μN in load and 1 nm in displacement, allow the measurement of sub-micron surface mechanical properties. For thin surface coatings this is particularly important, to minimise the influence of the underlying substrate. A typical curve is shown in §3.2.5.

Experimental (Vito):

The measurements were carried out using a NanoTest 550 instrument manufactured by Micro Materials Ltd. A trigonal pyramid (Berkovich) diamond indenter was used.

Analysis of the indentation curves was carried out following the method proposed by Oliver and Pharr [OLI 92]. A more elaborate description of the followed calculation method for the hardness and Young's modulus is given in the 12 month progress report of Vito in annexe A.

The test-parameters used were as follows:

Table 2.2-1: DSI test parameters.

max. depth	500 nm
initial load	0.05 mN
loading/unloading rate	1 mN/s
distance between indents	50 μm
drift acquisition time	30 s
hold time at max. load	10 s

Ten indents per specimen were performed, and outliers were rejected following ASTM Standard E 178-80. At least 5 measurements per specimen were used for the calculations.

2.2.6 Electron probe microanalysis (composition)

EPMA is a technique used to determine the elemental composition of a specimen by detecting characteristic X-rays generated in the specimen by interaction with an electron beam. The X-rays are analysed using a solid state detector according to their energy (EDXA: Energy Dispersive X-ray Analysis), or using diffraction crystals according to their wavelength (WDXA: Wavelength Dispersive X-ray Analysis). The latter method allows to analyse the characteristic X-ray spectrum with greater resolution.

Experimental (Vito):

Analytical apparatus: JEOL SUPERPROBE JXA-8621.

Off-line matrix correction software: STRATA v5.0.

Depending on the nature of the coatings, different electron beam voltages and currents were used. WDXA was chosen for all analyses.

Qualitative analyses, quantitative analyses and (elemental) line scans were applied to all the specimens in order to identify the elements present, to determine the composition and to check the homogeneity of the coatings, respectively.

2.2.7 Auger spectroscopy (composition)

Auger spectroscopy is used for compositional analyses in the surface layer of solid materials. The information depth from where Auger electrons are provided is typically 3 nm. Consequently, only the first atomic layers of the material can be investigated. This is particularly interesting for studying the oxidation or corrosion phenomena. Combined with ionic etching, depth profiling can be done. The composition of very shallow layers, like interface layers between substrate and coating can be determined by AES depth profiling. The elements H and He can not be detected by AES. Furthermore, the accuracy is rather low ($\pm 30\%$ for quantitative analysis), except if a standard with a composition close to the sample is available.

2.2.8 Bending beam stress measurements

The presence of stresses in a coating on a thin substrate will cause the substrate to bend elastically. Measurement of the substrate bending is a common method for determining the stress in a coating. With the substrate touching the table, a concave surface indicates that the stresses in the coating are tensile, and vice versa. For a thin coating on a relatively thick substrate (thin film approximation [CHI 92]), the stress in the film, σ , can be calculated from the deflection of the free end of the strip, δ , using the simple Stoney equation:

$$\sigma = \left(\frac{E}{1-\nu} \right)_s \frac{t_s^2}{3L^2 t_c} \delta \quad (2.2-1)$$

where $(E/1-\nu)_s$ is the biaxial modulus of the substrate, t_s and t_c are the thicknesses of the substrate and the coating, respectively, and L is the length of the strip. This equation is only applicable if the width-to-length ratio of the substrate is smaller than approx. 1/5.

Experimental:

Alkali zinc borosilicate glass strips (thickness code 0 = 85 to 130 μm) with dimensions of approx. 5 mm x 50 mm are used. The Young's modulus, E , Poisson's ratio, ν , and thermal expansion coefficient, α_m , for this material are 74.5 GPa, 0.22 and $7.4 \cdot 10^{-6}$ /K, respectively. A thin coating (usually < 500 nm) of the material under investigation is deposited on the glass strip, to prevent breaking of the thin glass strip. To determine the deflection of the free end of the strip, it is taped at one end onto an optical flat, and the distance between the other end of the strip and the surface of the optical flat is measured using a eye-piece lupe with measuring scale.

2.2.9 XRD Stress measurements

X-ray diffraction offers an in situ observation of the elastic strain of the crystal lattice close to the surface of polycrystalline materials. The lattice strain is measured in several directions. The strain tensor, characteristic of the sampled material, can then be derived. From the strain tensor, the stress state can be calculated with the aid of elastic constants.

Experimental

Phase identification was done by a coupled θ - 2θ measurement (Cu) on a Siemens D5000 machine in a Bragg-Brantano configuration. The measurement was done between 30° and 150° with step 0.02° (8 sec/step).

Stress measurements were done with an uncoupled θ - θ Philips diffraction apparatus with thin film attachment (Co). The stress measurements were based on a Reuss approach (constant stress).

Measurements for Zn were done by d - $\sin^2\psi$ method on the $\langle 112 \rangle$ plane. Step was 0.3° while the measuring time was variable (criterion: signal/noise ratio had to be at least 50). The diffraction slit was 0.25° .

The LIBAD method was used for the TiN measurements. The method is discussed in detail in [ACK 94]. The major aim of this method is to gain as much diffracted intensity from the coating as possible. Therefore, the X-ray beam enters the sample under a low angle α , let say between 0.6 and 5° . The angle α is fixed. However, the strain has to be measured in several directions of ψ . This is achieved in the LIBAD method by scanning the 2θ angle of several (hkl) planes instead of one single plane as in the d - $\sin^2\psi$ method. With this method the incident angle is kept constant while all peaks are scanned.

The step and measuring time were chosen in such a way that a signal/noise ratio of at least 75 was reached. The diffraction slit was 0.25° . The incident angle was chosen in such a way that only the upper part ($1 \mu\text{m}$) of the coating was measured.

2.2.10 Raman spectroscopy (DLC structure)

Raman spectroscopy is an analytical technique that yields information about the molecular structure of materials. The specimen under investigation is being irradiated with a strong, monochromatic light source (focused laser beam). The radiation scattered by the specimen is analysed by means of a monochromator. The energy loss or gain of photons with respect to the incident radiation is equivalent to the difference between two vibrational energy states of Raman active molecules in the material under investigation.

Experimental:

A DILOR XY800 confocal macro Raman instrument was used.

Ar-laser wavelength: 514.5 nm ;

laser spot diameter: $100 \mu\text{m}$;

laser power: 100 mW ;

gratings: 1800 mm^{-1} ;

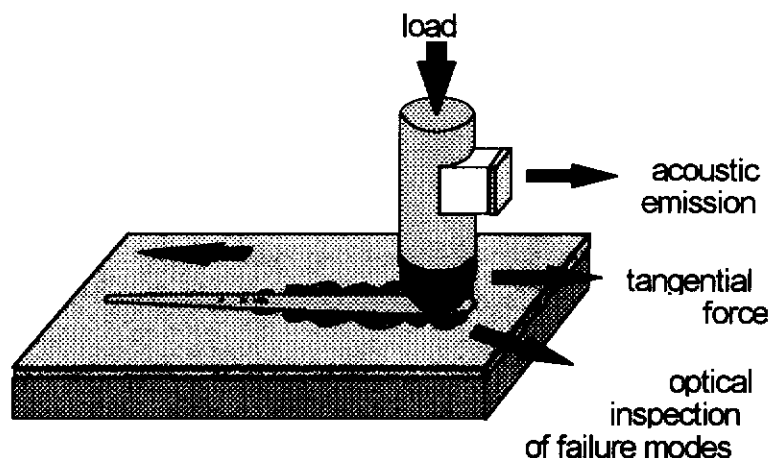
wavenumber range: $450 - 2000 \text{ cm}^{-1}$.

Three scans per specimen were recorded.

2.3 Theoretical principles of adhesion tests

2.3.1 Scratch Adhesion Test

The conventional scratch test consists of drawing a diamond stylus across the surface under increasing normal load, until some well defined failure event is observed in a regular fashion along the scratch track (Fig. 2.3-1). The normal load at which this occurs is called the critical normal load L_c (unit: N). The failure event is determined by inspection of the scratch track under a microscope, after the scratch has been made. When the coating fails by spallation from the substrate, the corresponding critical load is considered to be relevant as a measure of adhesion.



Scratch test

Fig. 2.3-1 Schematic representation of conventional progressive loading scratch test.

The scratch test method can be operated in the following 3 operation modes:

- **Single pass conventional progressive loading scratch test (SPST):** by applying a load ramp to the scratch stylus during the displacement of the specimen underneath it.
- **Single pass operation at constant loads (CLST):** by the stepwise increasing of the normal load between successive scratches carried out under constant load at different locations on the specimen surface.
- **Multipass operation at constant sub-critical load (MPST):** by the repeated scratching under a constant sub-critical load within the same scratch track.

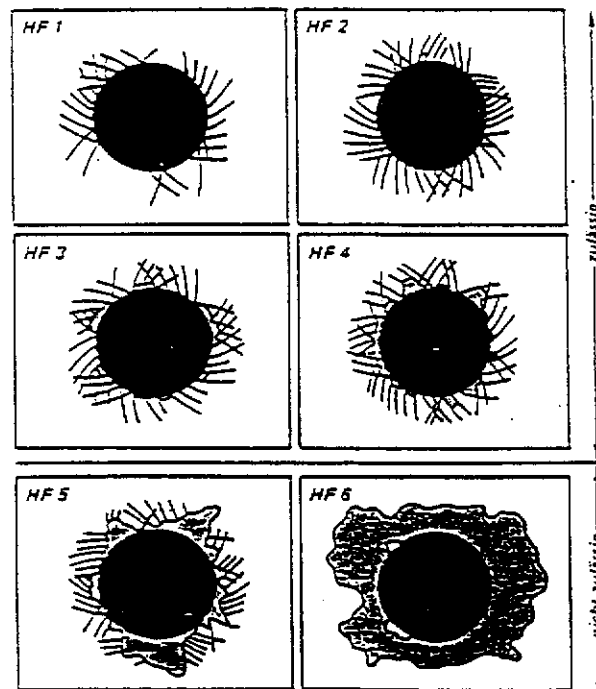
The SPST mode is used for the first order assessment of critical loads corresponding to major coating damage failure, while the CLST mode allows the statistical damage analysis of coatings along their surface. Finally, the MPST mode subjects the coated surface to a low-cycle fatigue type contact, which is considered to better simulate real working conditions of coated components. These three operation modes have been explored within the framework of this research programme.

For the first two modes, guidelines of test are described in the European pre-Standard ENV 1071-3:1994 'Determination of Adhesion by the Scratch Test'.

As for other engineering adhesion test methods, 'adhesion values' (critical loads) obtained by scratch testing depend not only on basic adhesion, *i.e.* the interfacial bond strength, but also on other coating/substrate composite properties (hardness, modulus, roughness, friction and coating thickness). As a consequence, the scratch test can at best be a semi-quantitative assessment of coating/substrate adhesion: if performed with care, the technique can repeatedly enable the ranking of the adhesion properties of a number of similar coating/substrate composites.

2.3.2 Rockwell Indentation Adhesion Test

In this test, the coated surface is indented with a diamond Rockwell C indenter causing damage to the coating close to the indent. The failure event is determined with a metallographic microscope (100x) and compared with the different failure classes shown in Fig. 2.3-2. This allows the coating/substrate adhesion to be classified from 'Adhesion Strength' AS1 to AS6.





 : crack network;
 : delamination

Fig. 2.3-2 Adhesion classes with the Rockwell indentation test.

The indentation is being performed following the European Standard EN 10109-1:1995, but the Rockwell indentation adhesion test on its own has not yet been the subject of standardisation. Test guidelines have been described in VDI-Richtlinie 3198-1991 and DIN Fachbericht 39-1993, p. 213.

2.3.3 Four Point Bending Adhesion Test

Fig. 2.3-3 shows the design of the four-point bending test.

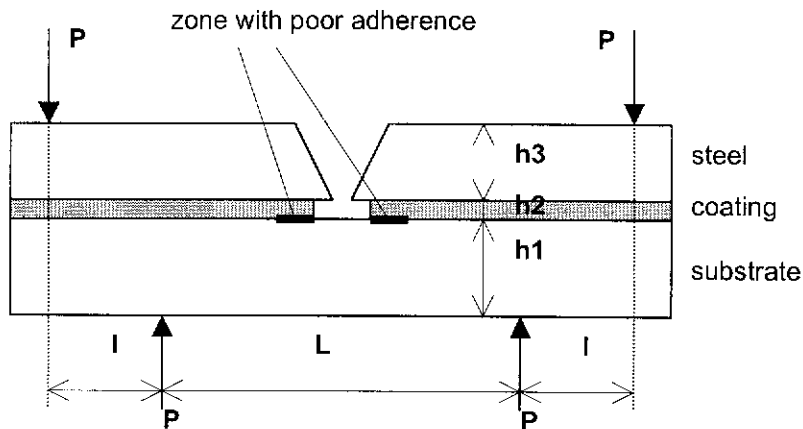


Fig. 2.3-3 Design of the four-point bending test.

Griffith's theory postulates that under a given loading, the crack is propagating if the total energy of the system decreases during the propagation. For an increase in crack size of dA , the crack will propagate if:

$$G_C dA \leq d(W - U_E) \quad (2.3-1)$$

with W = the potential energy of the external forces (Nm);
 U_E = the stored elastic strain energy (Nm);
 G_C = the critical energy release rate (N/m).

Under constant displacement:

$$\left. \frac{dW}{dA} \right|_P = 0 \quad (2.3-2)$$

P is the load (N). Equation 2.3-1 becomes now:

$$G_C = - \left. \frac{dU_E}{dA} \right|_P \quad (2.3-3)$$

For the crack located between the inner loading lines, the moment is constant. From the Euler-Bernoulli's beam theory, the stored elastic strain energy can be expressed in terms of applied moment M . G_C is given by equation 2.3-4.

$$G_c = \frac{M^2}{2B} \left(\frac{1}{E_1 I_1} - \frac{1}{(EI)_0} \right) \quad (2.3-4)$$

with $M = P \cdot l / 2$ (Nm);

$E_1 I_1$ = the flexional rigidity of the cracked beam (Nm²);

$(EI)_0$ = the flexional rigidity of the uncracked beam (Nm²);

B = the width of the beam (m).

The flexional rigidity can be expressed analytically by:

$$(EI)_a = E_1 I_1 + E_2 I_2 + E_3 I_3 + \frac{E_1 S_1 E_2 S_2 (h_1 + h_2)^2 + E_1 S_1 E_3 S_3 (h_1 + h_3)^2 + E_2 S_2 E_3 S_3 (h_2 + h_3)^2}{4(E_1 S_1 + E_2 S_2 + E_3 S_3)} + E_1 E_3 h_1 h_3 \frac{S_1 + S_2 + S_3}{E_1 h_1 + E_2 h_2 + E_3 h_3} \quad (2.3-5)$$

$$E_1 I_1 = E_1 \frac{B h_1^3}{12}$$

In plane strain conditions, the apparent modulus is larger and is given by:

$$E_{app} = \frac{E}{1 - \nu^2} \quad (2.3-6)$$

2.3.4 Tensile Adhesion Test

2.3.4.1 principle

The coated sample is subjected to an increasing tensile strain, causing the film to crack and break into segments as illustrated in Fig. 2.3-4.



Fig. 2.3-4 Schematic representation of the tensile test for multiple crack spacing.

Cracks are nucleated perpendicular to the tensile axis, x_1 , and change the stresses and strains in the neighbourhood. Shear stresses are developed in the vicinity of the interface, resulting from the difference in the axial displacement between the coating and the substrate (Fig. 2.3-5):

$$\tau(x_1) = 2\mu\gamma(x_1) \quad (2.3-7)$$

$$\gamma(x_1) = \frac{u_c(x_1) - u_s(x_1)}{g} \quad (2.3-8)$$

with μ is the shear modulus of the interface,
 $\gamma(x_1)$ the shear strain at the interface,
 $u_c(x_1)$ and $u_s(x_1)$ are the deformations in the coating and the substrate respectively,
 g is a characteristic length of the interface,
 x_1 is the co-ordinate along the interface with origin at the crack.

From the local force balance, a differential equation for the stress in the coating is developed:

$$\frac{d\sigma(x_1)}{dx_1} = \frac{1}{h} \tau(x_1) \quad (2.3-9)$$

where h is the coating thickness; the tensile stress is assumed uniform through the thickness of the coating.

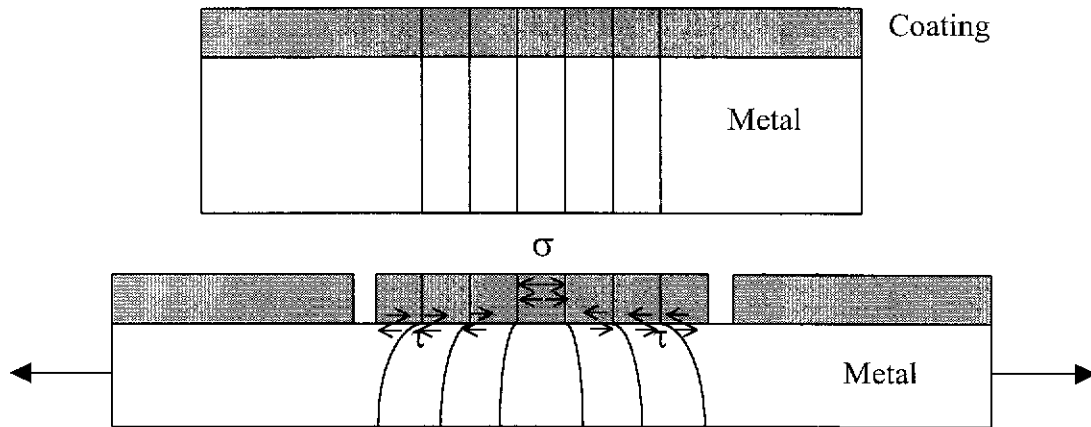


Fig. 2.3-5 Load transfer between metal and coating resulting from the difference in the axial displacement between the coating and the substrate.

The maximum shear stress, τ_{\max} , at the interface is obtained as:

$$\tau_{\max} = \frac{kh\sigma_f}{\lambda_{\max}} \quad (2.3-10)$$

with λ_{\max} is the maximum crack spacing,
 σ_f is the tensile strength of the film

k depends on the shear stress distribution along the interface, for which different models exist shown in next paragraph.

2.3.4.2 Models

Different forms have been assumed for the shear stress distribution $\tau(x_1)$, as illustrated in Fig. 2.3-6. Table 2.3-1 gives the values of k calculated for the different distributions and to be used in equation 2.3-10.

Table 2.3-1 The integration constant, k , for different shear stress distribution.

Reference	k
Tyson and Davies [TYS 65]	6
Kelly [KEL 66]	2
Agrawal and Raj [AGR 89]	π
Shieu [SHI 90]	π

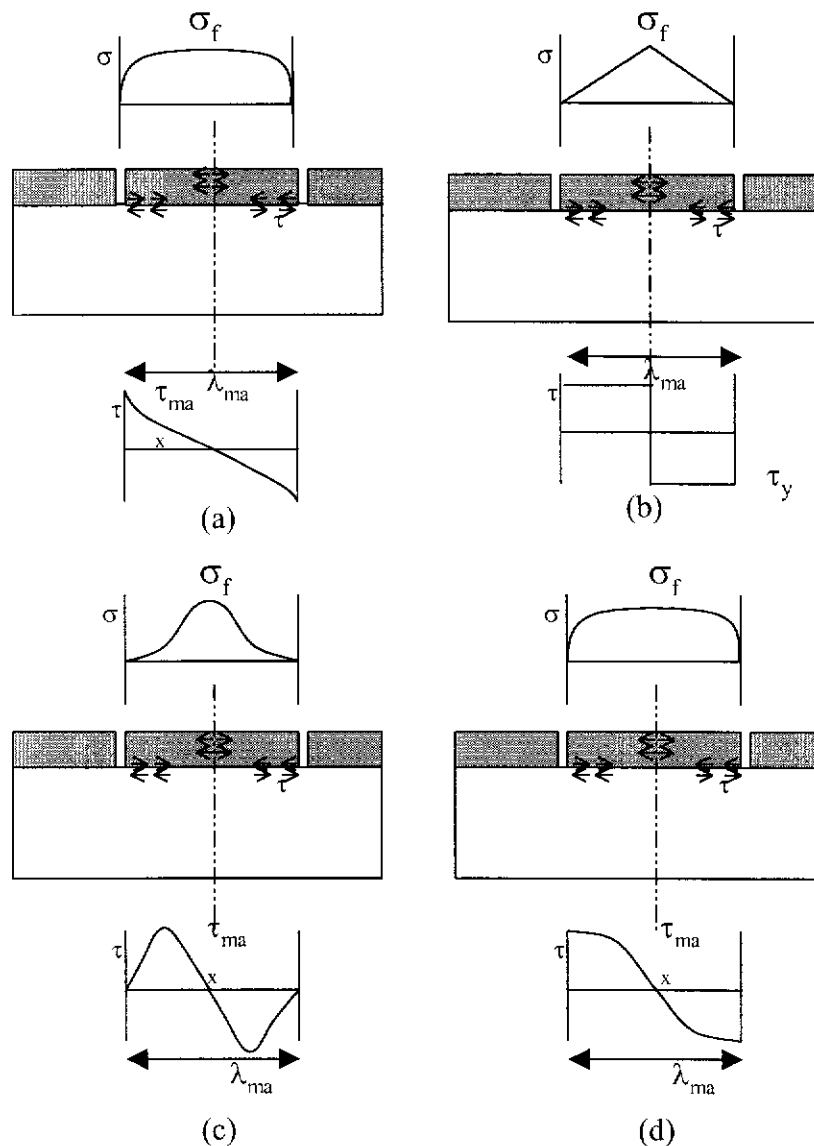


Fig. 2.3-6 Different models of the shear stress distribution along the interface between the metal and the coating, according to (a) Tyson and Davies (b) Kelly, (c) Agrawal and Raj, (d) Shieu.

2.3.4.3 Crack density distribution

The expected dependence of the crack spacing on the imposed strain is depicted in Fig. 2.3-7.

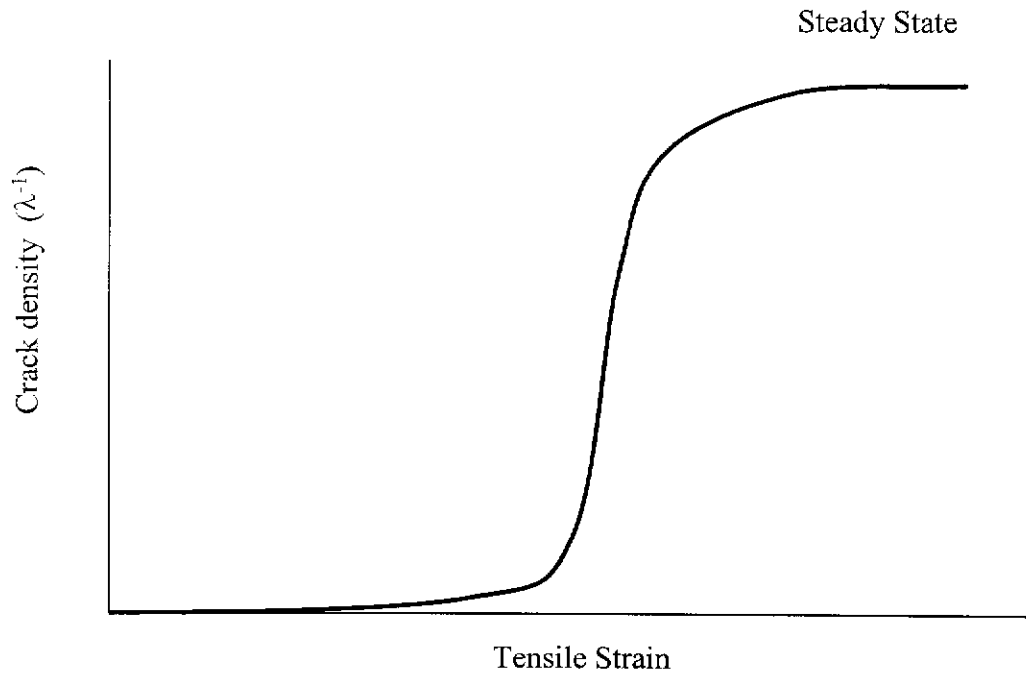


Fig. 2.3-7 Schematic plot of crack density as a function of imposed tensile strain.

The strain at which the cracks begin to appear, ε_f , gives a measure of the tensile fracture strength of the film.

$$\sigma_f = E_f * \varepsilon_f \quad (2.3-11)$$

Any residual stress initially stored in the coating should be added to the right-hand side of this equation.

In practice, the cracks will not be evenly spaced but have a statistical distribution due the brittle nature of the coatings . Even if the strength of the film were uniform everywhere, a spread of spacing covering a factor of two would be expected, from λ_{\max} to $\lambda_{\max}/2$. This factor reflects the extremes of a particular section of film either just breaking into two or just failing to do so. In fact, fracture of brittle materials is characterised by a strength distribution $F(\sigma)$ representing the fraction of failed specimens under loading σ [FRE 68]. For coating materials this function is obtained as a Weibull function.

$$F(\sigma) = 1 - \exp\left\{-\left(\frac{\sigma + \sigma^i - \sigma_f^0}{\sigma_f}\right)^m\right\} \quad (2.3-12)$$

$$F(\sigma) = 1 - \exp\left\{-\left(\frac{\sigma - \sigma_{th}}{\sigma_f}\right)^m\right\} \quad (2.3-13)$$

where $\sigma_{th} = \sigma_f^o - \sigma^i$ is the threshold value of fracture, σ_f^o and σ_f are the lower limit and the mean value of the strength, σ^i is the residual or internal stress and m , the Weibull modulus. The higher the value of m , the more homogeneous are the mechanical properties in the volume of the coating.

Ramsey et al. [RAM 91] as well as Henstenberg [HEN 89] used Monte Carlo simulations to determine the crack spacing distribution for a given value of the Weibull modulus, m , assuming interface sliding at a constant shear stress, governed by the shear yield stress of the metal, τ_y (Kelly model [KEL 66]). For example, the Monte Carlo simulations of Henstenberg [HEN 89] are showed in Fig. 2.3-8.

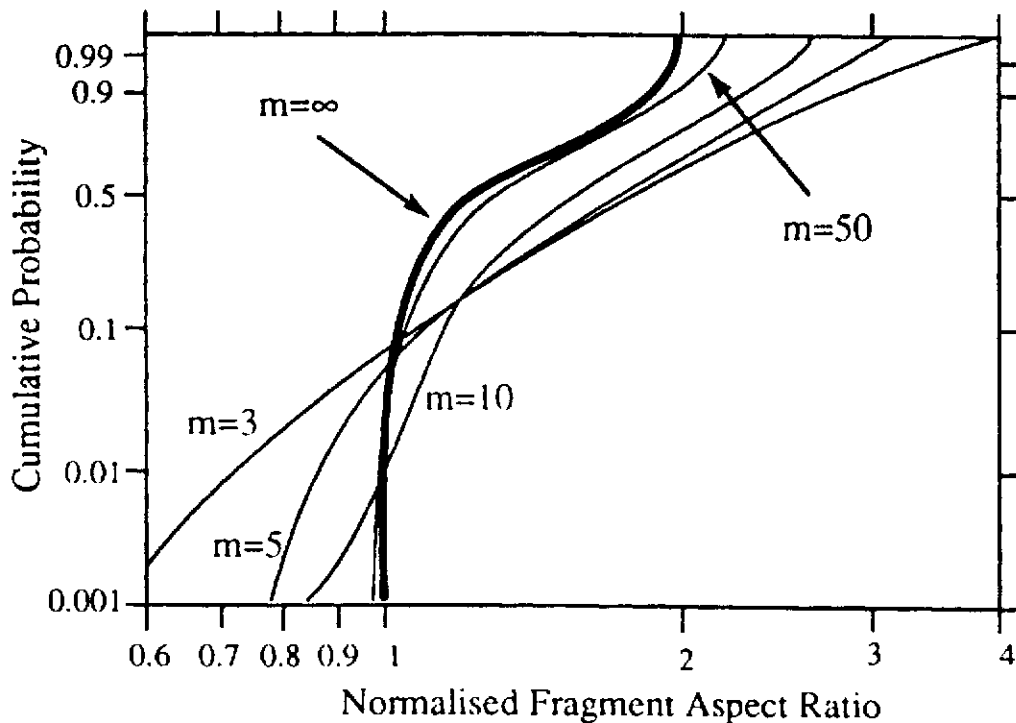


Fig. 2.3-8 Probability distribution functions for the aspect ratio of fragments, with several values of the Weibull modulus m , according to the Monte Carlo model of Henstenberg and Phoenix.

2.3.4.4 Film Decohesion

In some systems, film cracking may be accompanied by interface decohesion. Interface crack propagation is governed by the associated energy release rate, G_d . Once nucleated, the non-dimensional energy release rate initially diminishes with crack propagation length.

Fig. 2.3-9 illustrates the evolution of the energy release rate related to film decohesion as a function of the non-dimensional crack length. The increase in decohesion length with load may be used in conjunction with Fig. 2.3-9 [HU 89] to estimate the energy release rate G_d .

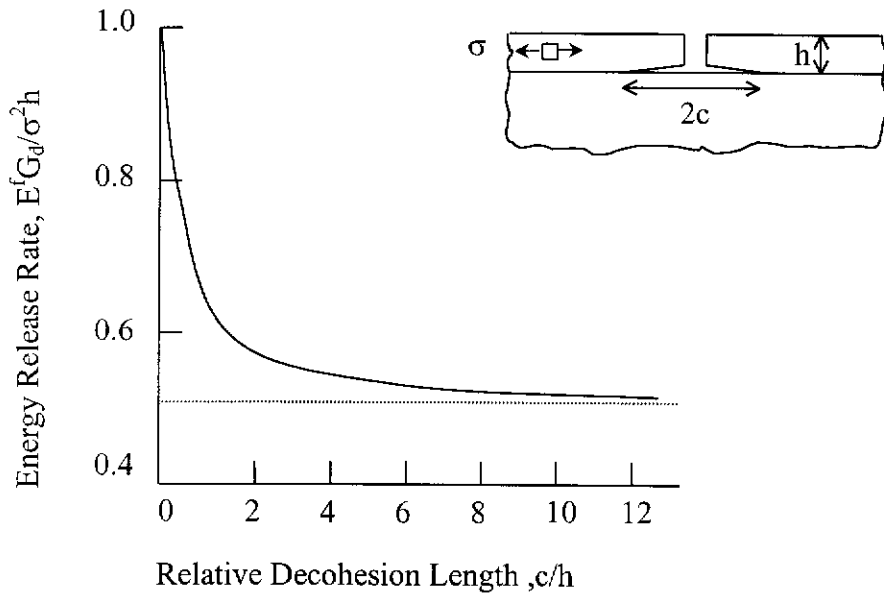


Fig. 2.3-9 Variations in the non-dimensional energy release rate with decohesion length for plane strain film decohesion in an elastically isotropic system.

Steady state condition develop for $c/h > 5$ with a phase angle of loading, $\Psi \cong 52^\circ$ [BOW 73]. Then, the energy release rate may be evaluated as [SUO 89],[GIL 84]:

$$G_d = \frac{1 - \nu^2}{2E_f} * \sigma_d^2 * h \quad (2.3-14)$$

This relation is only true if the crack front at the interface is long and if debonding does not interact with existing cracks.

In practice however, a scatter in the local properties leads to debonded regions of limited size and equation 2.3-14 and cannot be used to describe delamination in this simple form. Therefore, it is useful to estimate a threshold strain $\epsilon_{th,d} = \epsilon_d^0 - \epsilon_i$ for delamination as a measure of the material parameter ϵ_d^0 , a lower limit of the delamination strain. ϵ_i is the internal strain in the coating. The steady state delamination strain ϵ_d^0 may be related to the lower limit of the bonding energy γ by [GIL 83]:

$$\gamma = \frac{E_f}{2(1 - \nu^2)} (\epsilon_d^0)^2 h \quad (2.3-15)$$

Voronkin and al. [VOR 93] studied cracking and decohesion of amorphous hydrogenated carbon films on polymeric substrate by tensile testing. They suggest that a ratio of the area of fracture across the substrate to the whole film area should be used for quantitative estimation of adhesion:

$$A = \frac{S_1 - S_2}{S_1} \quad (2.3-16)$$

where S_1 is the mean width of the film fragment and S_2 is the mean size of the zone in which the delamination occurs at the film-substrate interface.

2.3.4.5 *Applicability*

To be valid, the test implies that the substrate deforms under stress with a greater displacement than the coating. The coating has therefore to be more brittle than the substrate. In the framework of this project, the test is used for TiN and DLC coatings on deformable automotive steel. The method was not applicable to hard steel substrates: the deformation of the substrate was too low to initiate cracks.

2.4 Adhesion Testing: Experimental Set-Up

2.4.1 Scratch test

A CSEM Revetest scratch tester was used.

Test parameters:

scratch stylus:	diamond Rockwell C (120° cone with 200 µm tip radius);
normal loading rate:	100 N/min.;
load range:	1* - 10 N for Zn; 5* - 100 N for TiN; 5* - 50 N for DLC;
table displacement rate:	10 mm/min.;
test atmosphere:	air with 50 ± 5% relative humidity.

* a start load different from 0 N was used to allow a better determination of the start of the scratch track.

The scratch tester has been operated in the 3 modes described in paragraph , namely:

- SPST: single pass conventional progressive loading
- CLST: single pass operation at constant loads
- MPST: multipass operation at constant sub-critical load

2.4.2 Indentation test

The indentations were performed by a Hoytom 1003A Rockwell tester.

For a Rockwell C measurement a sphero-conical diamond indenter is used with a 120° deg angle with a spherical apex of 0.200 mm (i.e. same indenter as in scratch test). A minimum load of 10 kg and a maximum load of 150 kg are used.

The influence of the following parameters was studied:

- the indentation load;
- the load rate;
- the hold time.

The influence of the indentation load was studied using the parameter of a standard Rockwell C, Rockwell A, Rockwell D and Brinell indentation test. In all tests the standard Rockwell C stylus (diamond cone, 120° angle) was used but with different loads: 150 kg, 60 kg, 100 kg and 187.5 kg respectively. In each case the time of indentation was held constant at 45'' (time interval between applying the major load and the end of the indentation test) and the indenter was held for 20'' in the sample to be tested.

To study the load rate i.e. the velocity at which the indentation was made a standard Rockwell C indentation (maximum load) was made. The indentation speed at the test apparatus can only be changed manually and readings of the actual speed are not available. Therefore the dial that controls the speed was set in its two extreme positions and in the middle position. Indentations were made in 3'' (fast), 130'' (slow) and 45'' (middle). Since no influence was noticed for the different indentation times (i.e. load rates) the latter was used as standard indentation time for all the other tests. The hold time was 20'' (standard hold time).

The standard Rockwell C test was repeated with a holding time of 5 and 60" respectively to test the influence of the hold time, i.e. to study the possible influence of time dependent deformation (creep, anelastic recovery).

Additional indentation tests were carried out with a standard scratch tester (CSEM-Revetest). The x-motor was blocked and indentations were made at 100 and 200 N. The load rate was 100 N/min.

2.4.3 Four-point bending

In the four-point bending test, the load is recorded as a function of the displacement. The curve is exhibiting a fall in the load when the crack propagates. The propagation load P_c is used to calculate the energy release rate. The displacement rate is small: 0.2mm/min.

The space (l) between the inner and the outer load lines (see Fig. 2.3-3) is 8mm. The overall dimensions of the specimens are 60mmX14mm. The space between the inner load lines (L) is 32mm. The total thickness of the samples depends on coating thickness (h_2) and is precisely measured.

In each case 5 measurements were carried out.

2.4.4 Tensile testing

The specimen (size 10 x 1 x 60 mm³) were mounted in an INSTRON tensile machine. Incremental strains were applied to the specimens using an Instron tensile tester with a constant displacement rate of the crosshead of 0.2 mm min⁻¹. The apparition of cracks was detected via in-situ micrography using replica after each increment. The segment length distribution between cracks was found using image analysis techniques coupled to an optical microscope.

3 RESULTS

3.1 Deposition of the Coatings: WP1

3.1.1 PACVD DLC (Vito)

The DLC coatings were produced in a capacitively coupled r.f. (13.56 MHz) PACVD process from a CH_4/H_2 precursor mixture. For variants A and B, the biasing conditions were controlled to produce coatings with good mechanical properties, but the adhesion between the coating and the substrate has been deliberately varied by changing the carbon content in the $\text{a-Si}_{1-x}\text{C}_x\text{H}$ adhesion interlayer (Fig. 3.1-1). A $\text{SiH}_4/\text{CH}_4/\text{H}_2$ gas mixture was used to produce this adhesion promoting interlayer. The adhesion properties of DLC to steel are sensitive to the carbon content in this adhesion interlayer [DEK]. When the carbon content is too high, the DLC coating spontaneously spalls off the substrate. Variant C was obtained by using the optimum adhesion interlayer as for variant A while decreasing the bias voltage during the subsequent deposition of the DLC layer, yielding a more polymer-like (soft) top coat.

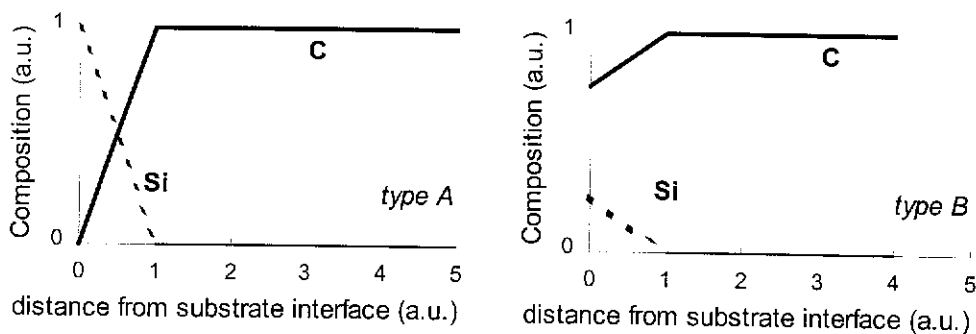


Fig. 3.1-1 Schematic representation of the interface structure of DLC coatings variants A and C (a) and variant B (b).

For the selection of the DLC variants, the coatings were deposited at low working pressures (2 Pa) to have optimum control of the interlayer structure. This resulted in relatively thin coatings ($\cong 1 \mu\text{m}$), however. For the work in task C it was decided that more realistic coating thickness are required (2 - 3 μm), and therefore the working pressure had to be increased to obtain coatings within an acceptable time scale (10 Pa, 350V/120min. for variants A and B; 60V/480min. for variant C (lower growth rate)). Using these latter deposition conditions, five $30 \times 30 \times 5 \text{ mm}^3$ specimens of each DLC variant were produced for the characterisation work in task B (NOR 682-A, NOR 684-C, and NOR 686-B). A slightly lower CH_4 to SiH_4 start ratio (19%) had to be used to prevent the thicker DLC variant B to spall off spontaneously from the substrate. During an intermediate coating run NOR 683, where a ratio of 21% was used, spontaneous spallation was indeed observed.

In the attempt to generate the dedicated defect required for the 4 point bend (4PB) 'crack propagation' test specimens used at ULB, a DLC variant A was deposited onto a series of the smaller $60 \times 10 \times 2 \text{ mm}^3$ specimens with line defects produced by a felt-tip pen, evaporated C and Au, and laser-oxidised lines of different energy inputs. All procedures except the Au evaporated line produced defects with sharp borders. However, the C-evaporation method turned out to be poorly reproducible, and therefore part of the defects were produced by a felt tip pen line, which represents in fact the quickest and simplest method to create the notch.

Table 3.1-1: Different specimen preparation with DLC coating for the 4PB technique.

run	DLC variant	substrates
NOR1169	A	4 60x10x2 mm ³ C60 steel with thick evaporated C line 2 60x10x2 mm ³ C60 steel with thin evaporated C line 4 60x10x2 mm ³ C60 steel with felt tip pen line 5 60x10x1 mm ³ C60 steel with felt tip pen line 5 60x10x1 mm ³ C60 steel without defect 5 60x10x1 mm ³ automotive steel without defect 10 30x30x5 mm ³ C60 steel
NOR1170	B	1 60x10x2 mm ³ C60 steel with thick evaporated C line 1 60x10x2 mm ³ C60 steel with thin evaporated C line 3 60x10x2 mm ³ C60 steel with felt tip pen line 2 60x10x1 mm ³ C60 steel with felt tip pen line 3 60x10x1 mm ³ C60 steel without defect 5 60x10x1 mm ³ automotive steel without defect 10 30x30x5 mm ³ C60 steel
NOR1176	C	1 60x10x2 mm ³ C60 steel with thick evaporated C line 1 60x10x2 mm ³ C60 steel with thin evaporated C line 3 60x10x2 mm ³ C60 steel with felt tip pen line 2 60x10x1 mm ³ C60 steel with felt tip pen line 3 60x10x1 mm ³ C60 steel without defect 5 60x10x1 mm ³ automotive steel without defect 10 30x30x5 mm ³ C60 steel

3.1.2 CVD TiN (WTCM)

After a cleaning step, including a solvent bath (+ ultrasonic agitation), an alkaline bath and a rinsing step, the specimens are mounted on a substrate holder. The deposition chamber is brought to a vacuum of 10^{-5} mbar.

For the coating type A (standard coating, good adhesion) the standard TiN at a deposition temperature of 450°C was chosen.

Coating type C is deposited at a lower temperature (200°C). Due to the changed deposition parameters compared to the standard TiN coatings, it is expected that these coatings have a different microstructure and therefore different properties. Despite this, coatings with good adhesion can be achieved.

For coating type B (standard coating, 'bad' adhesion) different sets of deposition parameters have been tried. At first this coating type was deposited after different polishing times of the substrates combined with different etching times during deposition. Since no reproducible coatings could be produced another series of tests was done. Hereby the thickness of the Ti intermediate layer was changed. It was found that coatings without a Ti intermediate layer gave coatings with good adhesion (which was not expected) but that the coating thickness was less than expected (1 μm or less after a 45' deposition). The hypothesis is that the coating flakes off several times during deposition (due to stress build up during deposition) and keeps growing again on the uncoated substrate material afterwards. The end result is a thin coating. The new type B coating that was selected had a Ti intermediate layer that was deposited without bias voltage whereafter a TiN coating was deposited with standard -150V bias voltage. Hereby the criterion of having an identical coating as coating A with different interface properties had been fulfilled.

For the bending tests a special specimen holder had to be developed since part of the substrate had to remain uncoated to introduce a crack.

Table 3.1-2: The specimens of type A, B and C for task C

batch	coating type	substrates
2556	A	5 60x10x3 mm ³ ASP23 steel with defect 5 60x10x1 mm ³ ASP23 steel without defect 5 60x10x1 mm ³ automotive steel without defect 10 30x30x5 mm ³ ASP23 steel
2551	B	5 60x10x3 mm ³ ASP23 steel with defect 5 60x10x1 mm ³ ASP23 steel without defect 5 60x10x1 mm ³ automotive steel without defect 10 30x30x5 mm ³ ASP23 steel
2544	C	5 60x10x3 mm ³ ASP23 steel with defect 5 60x10x1 mm ³ automotive steel without defect 10 30x30x5 mm ³ ASP23 steel

3.1.3 Electrodeposited Zn (ULB)

Fig. 3.1-2 shows schematically the continuous electrodeposition cell that is used.

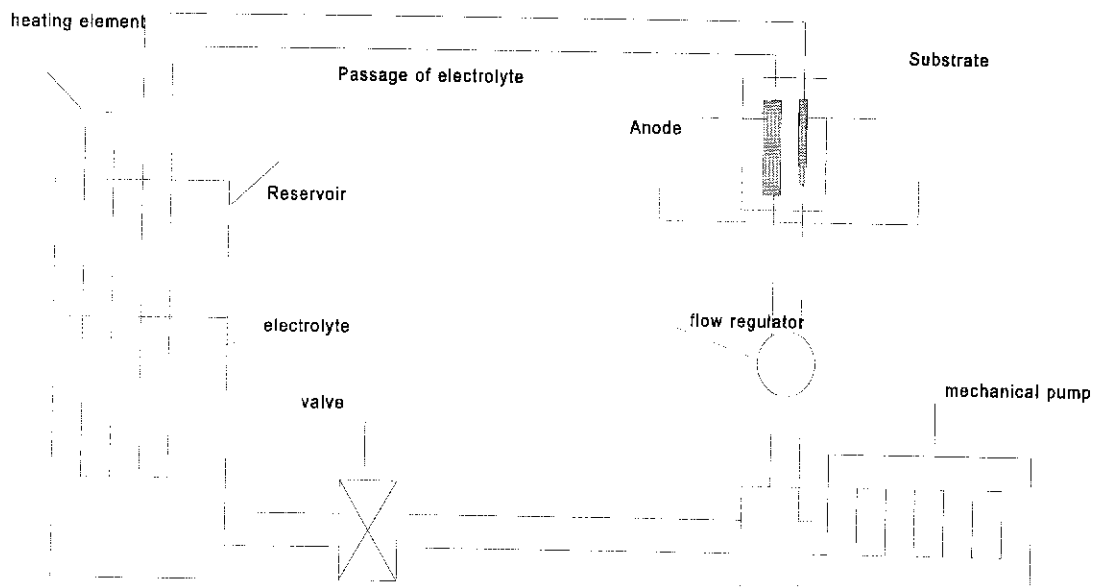


Fig. 3.1-2 schematic representation of the cell for the electrodeposition of Zn.

In order to obtain the Zn films with different adhesion properties, three Zn films are deposited on steel sheets, with a deposit thickness about 50µm, by varying the current density or by modification of the steel surface preparation. The preparation parameters are summarised in table 3.1-3.

Table 3.1-4: Deposition conditions and characteristics of Zn films. The composition of electrolyte is (5g H₂SO₄ +161 g Zn)/l.

Sample	Type	Preparation	Current Density (A/dm ²)	Electrolyte flow rate (m/s)	Temperature (°C)	Thickness of the coating (µm)
Zn35	A	#500	75	2	25	50
Zn36	B	#500 + 2h in FeCl ₃ (1w%)	75	2	25	55
Zn37	C	#500	100	2	25	60

The substrates are manually polished with #500 abrasive to obtain an arithmetic roughness of about 0.3µm according to DIN 4768. Then, they are degreased with alcohol. The middle part of the sheets is protected from polishing and degreasing with tape in order to obtain poor adherence locally, necessary for the four point bending test.

To produce the type B film (standard coating with poor adhesion), the steel sheet has been immersed in a FeCl₃ solution for two hours to obtain a homogeneous oxide layer on the sheet before deposition of the coating.

3.2 Characterisation: WP2

3.2.1 Introduction

The results shown below only concern the last series of coatings deposited, used in task C.

3.2.2 Coating thickness

The coating thickness has been measured both by the crater grinding technique and the measurement of cross sections in the SEM. The coating thickness was measured by the SEM at 5 different locations on the same cross section. The results are summarised below:

Table 3.2-1: Thickness results measured by the Calo test .

Coating type - variant	Thickness t [μm] avg. \pm st.dev.
DLC - A	2.12 ± 0.01
DLC - B	2.11 ± 0.17
DLC - C	1.53 ± 0.03
TiN - A	3.68 ± 0.03
TiN - B	3.29 ± 0.05
TiN - C	2.52 ± 0.03

The thickness of the ULB specimens could not be measured by the Calotest. The Zn coating is much thicker than the TiN and DLC coatings which means that the Zn coating was not penetrated even after prolonged crater grinding. The Zn also has a tendency to smear out which makes it more difficult to distinguish the border between the substrate and the coating. Moreover, both substrate and coating have the same colour. The thickness of the Zn coatings was measured on a cross section by optical microscopy (Table 3.2-2).

Table 3.2-2: Thickness results measured by the OM.

Coating type - variant	Thickness t [μm] avg. \pm st.dev.
Zn - A	45.0 ± 2.0
Zn - B	44.7 ± 1.5
Zn - C	48.0 ± 2.0

On a special batch of TiN and DLC coatings the thickness measured by Calotest was compared to the thickness measured by SEM on the cross section (Table 3.2-3). For the crater grinding test the measurements carried out at 5 different locations, for the SEM measurements the coating thickness was measured at 5 different locations on the same cross section.

Table 3.2-3: Comparison of thickness measurements with Calotest and SEM

		Avg.	St. dev.
DLC-A	Calo (μm)	2.31	0.09
	SEM (μm)	2.95	0.04
DLC-B	Calo (μm)	2.4	0.2
	SEM (μm)	3.16	0.04
DLC-C	Calo (μm)	0.9	0.2
	SEM (μm)	1.77	0.08
TiN A	Calo (μm)	4.1	0.4
	SEM (μm)	4.67	0.02
TiN B	Calo (μm)	4.4	0.2
	SEM (μm)	4.2	0.2
TiN C	Calo (μm)	3.0	0.2
	SEM (μm)	4.1	0.2

3.2.3 Surface roughness

The measurements were done under the following conditions:

Table 3.2-4: roughness measurement parameters.

coating - variant	cutoff length (mm)	evaluation length (mm)	traversing length	traversing length	data density Vito (data/mm)
			Vito + WTCM (mm)	ULB (mm)	
DLC-A	0.08	0.40	0.56	1.4	5000
DLC-B	0.08	0.40	0.56	1.4	5000
DLC-C	0.08	0.40	0.56	1.4	5000
TiN-A	0.25	1.25	1.75	2.25	1400
TiN-B	0.25	1.25	1.75	2.25	1400
TiN-C	0.08	0.40	0.56	1.4	5000
Zn-A	0.8	4.0	5.6	5	500
Zn-B	0.8	4.0	5.6	5	500
Zn-C	0.8	4.0	5.6	5	500

Vito: tracking force=0.7mN (approx.), stylus tip radius=5 μm .

WTCM: tracking force=0.9mN (approx.), stylus tip radius=5 μm .

ULB: tracking force=0.1mN (approx.), stylus tip radius=12.5 μm .

Each time 5 measurements were done.

The following results were obtained (Table 3.2-5):

Table 3.2-5: Roughness results

		WTCM		Vito		ULB	
		Avg	St. dev.	Avg	St. dev.	Avg	St. dev.
DLC - A	Ra	0.007	0.001	0.008	0.000	0.0035	
	Rz	0.047	0.011	0.051	0.003	0.0104	
	Rmax	0.060	0.014	0.064	0.006	0.0200	
DLC - B	Ra	0.006	0.000	0.007	0.000	0.0026	
	Rz	0.046	0.004	0.047	0.001	0.0097	
	Rmax	0.049	0.003	0.058	0.003	0.0197	
DLC - C	Ra	0.006	0.001	0.007	0.000	0.0040	
	Rz	0.052	0.007	0.045	0.001	0.0130	
	Rmax	-	-	0.064	0.006	0.0350	
TiN - A	Ra	0.063	0.004	0.041	0.003	0.0320	0.0027
	Rz	0.483	0.054	0.338	0.016	0.2072	0.0340
	Rmax	0.581	0.125	0.391	0.028	0.3094	0.0800
TiN - B	Ra	0.049	0.002	0.039	0.003	0.0294	0.0035
	Rz	0.438	0.037	0.346	0.018	0.0828	0.0428
	Rmax	0.759	0.171	0.412	0.051	0.1420	0.0629
TiN - C	Ra	0.014	0.006	0.008	0.001	0.0056	0.0033
	Rz	0.225	0.094	0.057	0.007	0.0432	0.0271
	Rmax	0.551	0.413	0.070	0.009	0.0473	0.0350
Zn - A	Ra	0.85	0.14	0.879	0.128	1.08	
	Rz	5.70	0.94	5.947	0.508	4.52	
	Rmax	7.30	1.45	7.908	0.850	5.92	
Zn - B	Ra	1.12	0.20	1.272	0.072	0.91	
	Rz	7.45	1.59	8.493	0.749	4.62	
	Rmax	8.94	1.90	11.217	0.701	7.10	
Zn - C	Ra	1.08	0.09	1.453	0.162	1.21	
	Rz	7.57	0.44	9.401	0.910	5.76	
	Rmax	10.42	1.20	12.252	1.876	8.40	

Note that the surface roughness values measured at ULB are systematically lower than those measured at WTCM and Vito, and that the differences become less for higher surface roughness. These observations can be easily explained by the different tip radii of the contact profilometers, i.e. 12.5 μm in the case of ULB and 5 μm in the case of Vito and WTCM.

Also remarkable is the increase of the surface roughness of the Zn films with the current density. This is probably due to hydrogen release.

3.2.4 Composite hardness

The following overall hardness has been measured (Table 3.2-6):

Table 3.2-6: results of the composite hardness measurements according to the method of Rockwell C.

		Avg	St. dev.	Max	Min
DLC - A	HRc	59.3	0.5	60	59
DLC - B	HRc	59	0	59	59
DLC - C	HRc	59.8	0.5	60	59
TiN - A	HRc	63.9	0.6	64.5	63
TiN - B	HRc	65	0	65	65
TiN - C	HRc	65	0	65	65
Zn - A	HRc			76	70
	HRa	35	2	37	32
Zn - B	HRc			78	70
	HRa	34	2	36	31.5
Zn - C	HRc			75	74
	HRa	35	1	36	34

As can be seen are the Rockwell C measurements for the Zn specimens extremely high. These values are even out of the standard Rockwell C range. This is due to the thin and soft substrate and coating material. For thin materials Rockwell A (same diamond indenter, major load 60 kg) measurements are more appropriate. These values can be found in the above table.

3.2.5 Coating hardness and Young's modulus

Table 3.2-7: Results of the nanoindentation.

Coating type - variant	Hardness H [GPa]	Modulus E [GPa]
	avg. ± st.dev.	avg. ± st.dev.
DLC - A	18.9 ± 0.5	150 ± 2
DLC - B	19.8 ± 0.8	158 ± 2
DLC - C	5.6 ± 0.2	69 ± 2
TiN - A	31 ± 6	291 ± 33
TiN - B	29 ± 6	266 ± 25
TiN - C	26 ± 2	257 ± 6
Zn - A	0.8 ± 0.1	114 ± 17
Zn - B	0.9 ± 0.1	124 ± 26
Zn - C	0.8 ± 0.1	107 ± 17

The averaged indentation hysteresis curves, in each case together with that of the reference Si(111) specimen, are shown in Fig. 3.2-1.

displacement vs. load hysteresis curves

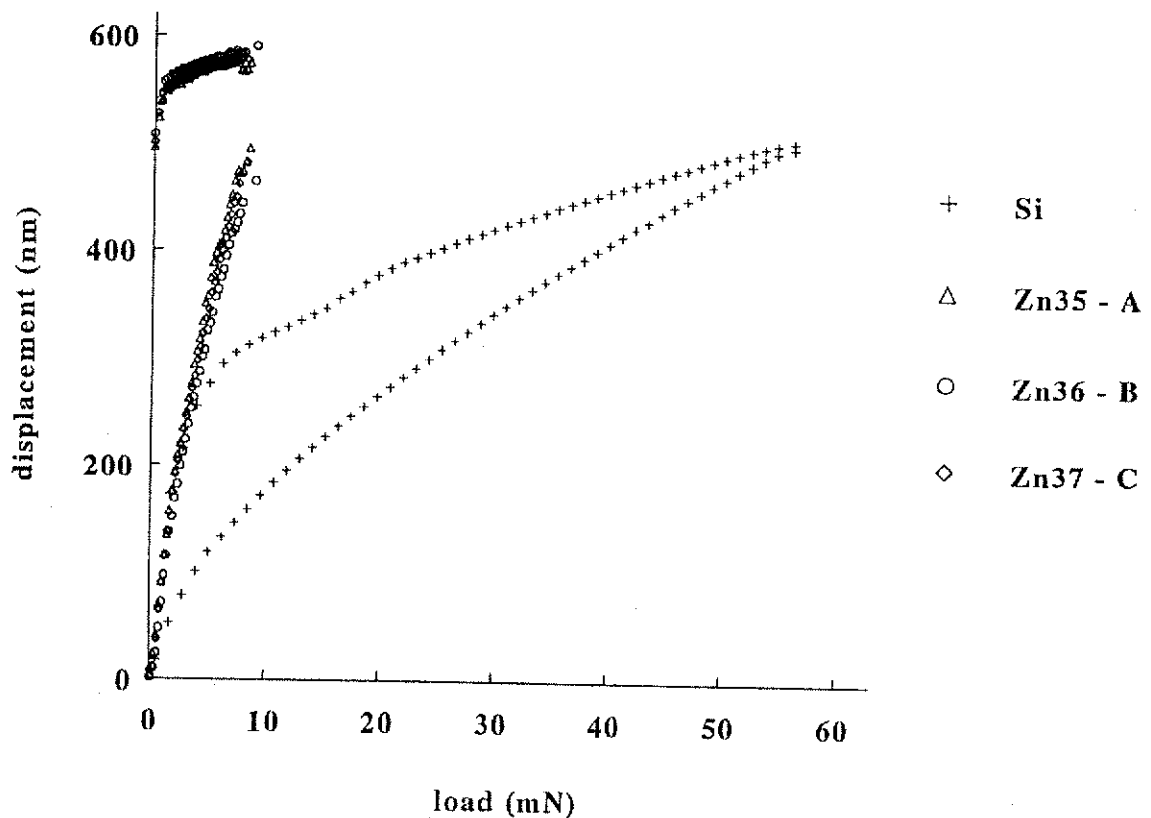


Fig. 3.2-1: Indentation hysteresis curves for Zn, TiN and DLC variants, and the Si reference.

Within the error margins, the mechanical properties of all three Zn variants agree with each other. The modified Zn coating (variant C) is thus, from the mechanical point of view, not different from the standard coatings (A/B). The DSI measurements were done on mirror polished samples supplied by ULB. Note the considerable creep occurring during the 10 s hold period at maximum load.

The high surface roughness of the TiN variants A and B resulted in large scatter of the measured mechanical properties. This can be explained by the fact that indents at roughness peaks result in compliant contacts and vice versa, indents in roughness valleys result in stiff contacts. As a rule of thumb, the surface roughness parameter R_a should be one tenth of the maximum indentation depth. Within the large error margins, the values for both coatings agree, but the indentation curves indicate that the mechanical properties of both standard TiN coatings (variants A/B) are different. The apparent aberrations in the TiN curves at peak loads stem from the averaging procedure adopted: displacement values are averaged for different load intervals, which results in these aberrations for dispersed individual curves. TiN variant C yields lower hardness and Young's modulus values, and the scatter on these values is significantly lower due to its smoother surface.

The mechanical behaviour of the three DLC variants was as expected. The standard DLC variants A and B show identical indentation curves, while the polymer-like variant C is considerably softer and more elastic.

3.2.6 Composition

The qualitative and quantitative analyses by EPMA demonstrated that the a-C:H and Zn coatings contained only the constituent element. A small amount of oxygen was found in the TiN coatings. The line scans (five for each specimen) illustrated that all coatings are homogeneous. The length of each line scan was 10 mm, which corresponds to that of a typical scratch track. Details are given in the 12 month report of Vito.

It was clearly shown by AES that the Si content at the coating-substrate interface for variant DLC-B was significantly lower than for variants A and C, as expected. Indeed the lower Si-content was intentionally created to produce poor adhesion properties (Fig. 3.2-2).

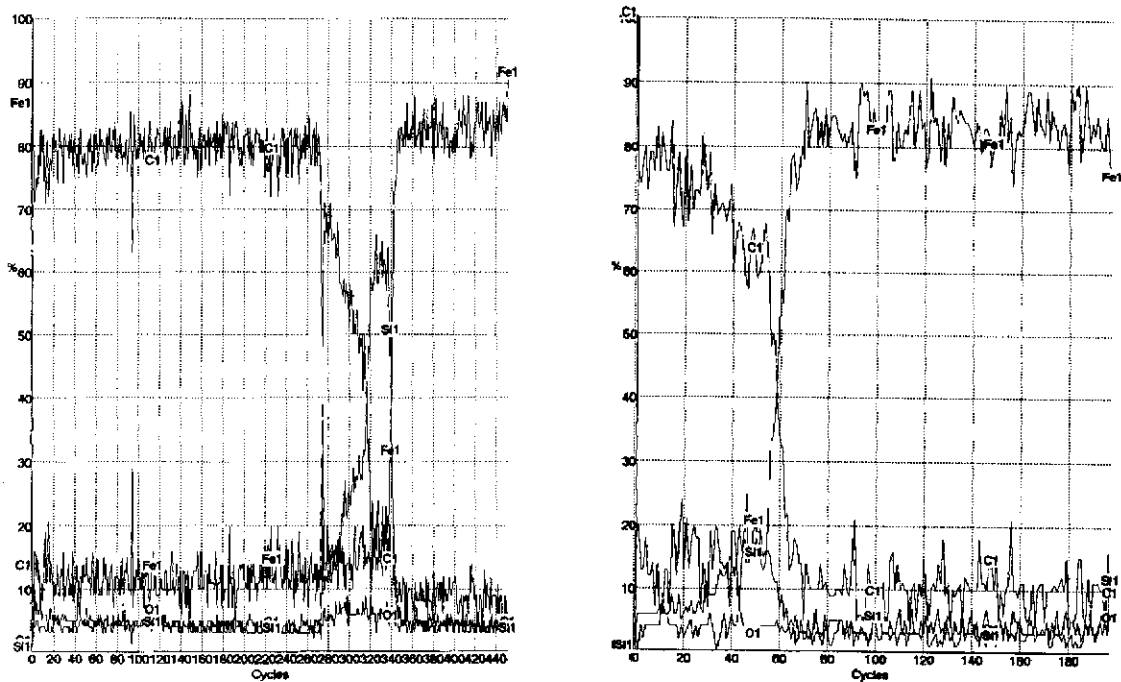


Fig. 3.2-2 Concentration profile by AES of DLC-A and DLC-B coatings.

3.2.7 Coating microstructure and morphology

The specimens were cooled in liquid nitrogen and then broken. The broken sections were looked at by scanning electron microscopy. The photographs and details are included in the 12 month report of WTCM the 2nd 12 month report of WTCM.

The microstructure of the TiN coatings is columnar, while the Zn coatings show more equiaxed grains which have a smaller size near the interface with the substrate. This is confirmed by optical microscopy on cross-sections of the Zn coatings. Furthermore, the high current density crystallites are smaller than those obtained at low current density.

Additionally, the surface morphology of the TiN coatings is studied by optical microscopy and of the DLC coatings by AFM (insulating coating).

The AFM image of the surface of the DLC films shows polishing marks on all the specimens. The sample A and C surfaces exhibit protrusions. This could be due to dust arising from the specimen cutting operations.

The optical micrographs of the TiN surface morphologies demonstrated that the type A and B surface morphologies are quite similar, while the type C film presents a distinct morphology (smaller globules).

The SEM micrograph of the surface of the Zn films revealed that the surface quality of these films seems constant. Nevertheless, the type C Zn coating presents smaller crystallites due to higher deposition current density. The photographs are given in the 12 month report of ULB.

3.2.8 Internal stress

3.2.8.1 Bending beam stress measurements on DLC

Thin films of DLC variants A (= B, because another interlayer is used here) and C were deposited onto the glass strips (three for each), without a-Si_{1-x}C_x:H adhesion interlayer to determine the stress in the DLC top layers only. The results are shown in

Table 3.2-8: Internal stresses in the DLC variants.

coating run	DLC variant	thickness μm	stress GPa
NOR878	A/B	0.35	- 1.9
	A/B	0.35	- 2.0
	A/B	0.35	- 1.95
NOR879	C	0.23	- 1.07
	C	0.23	- 1.05
	C	0.23	- 1.28

As expected, the stresses in both coatings were compressive in nature, and the stress in the polymer-like coating was considerably lower than in the diamond-like carbon coating (-1.13 ± 0.13 GPa compared to -1.95 ± 0.05 GPa).

It must be noted that it is impossible to perform XRD stress measurements on the DLC coatings because of the amorphous character of this coating.

3.2.8.2 Bending beam and XRD stress measurements on TiN

To compare the bending beam method with the XRD methods used by the other partners, such a glass strip was coated with a thin TiN variant A layer by WTCM (run 2391). The reported thickness of this layer was: 0.3 μm (Calotest), and 0.25/0.27/0.22 μm (Fischerscope). In this case, however, a Ti interlayer was deposited prior to the TiN film. The reported thickness include the thickness of the interlayer.

Using equation (2.2-1), and assuming a TiN coating thickness of 0.25 μm, the stress in the coating was calculated as -4.13 GPa. To enable the comparison with the XRD measurements, however, one has to correct for the different thermal stresses in the coating induced by the different substrate materials, i.e. glass in the case of the bending beam method, and M2 steel in the XRD method.

The thermal stress induced in a coating due to the thermal expansion mismatch with the substrate can easily be calculated from:

$$\sigma_{th} = \left(\frac{E}{1-\nu} \right)_c (\alpha_{th,c} - \alpha_{th,s}) (T_{deposition} - R.T.) \quad (3.2-1)$$

One can use literature values for the elastic constants of TiN and M2 steel: $E_{TiN} = 450$ GPa; $\nu_{TiN} = 0.3$; $\alpha_{th,TiN} = 9.4 \cdot 10^{-6}/K$; $\alpha_{th,M2steel} = 11.7 \cdot 10^{-6}/K$ or measured elastic moduli. Indeed the elastic properties are measured by DSI at Vito ($E_{TiN} = 360$ GPa). This last option is preferable, because there is a wide dispersion in literature values for TiN moduli. These measured moduli are also used to convert the measured strains by the XRD methods into internal stress. For ν_{TiN} we assumed that it is 0.3. The deposition temperature was 450 °C.

It was calculated with the measured Young's modulus for the coating and the literature values for the other parameters, that the glass substrate induces a tensile stress of 0.43 GPa in the TiN coating, while the M2 steel substrate generates a compressive stress of -0.50 GPa in the coating. A comparison of the coating intrinsic stresses is made in Table 3.2-9. The results obtained by the two different techniques are comparable.

Using a more complex equation instead of eq. (2.2-1), to improve the accuracy of the calculation, does not help. For example, if the Senderoff equation is used,

$$\sigma = \frac{\left(\frac{E}{1-\nu} \right)_s \left(t_s + \frac{E_c(1-\nu_s)}{E_s(1-\nu_c)} t_c \right)^3}{3L^2 t_s t_c} \delta \quad (3.2-2)$$

which is better suited for the relatively large strip deflections (typically 1 to 3 mm), the total stress in the TiN coating (thermal + intrinsic) becomes -4.3 instead of -4.1 GPa. The intrinsic stress measured by the bending beam method now becomes - 4.73 GPa.

Table 3.2-9: Intercomparison of stress in TiN-A coating measured by different techniques/partners.

method	total stress in the coating GPa	coating intrinsic stress GPa	coating intrinsic stress (Senderoff) GPa
bending beam (Vito)	- 4.1	- 4.53	- 4.73
XRD (WTCM/IMO)	- 5.2	- 4.7	- 4.7
XRD (ULB)	- 4.6	- 4.1	- 4.1

For the TiN-B and TiN-C coatings we only obtained results with the XRD method (Table 3.2-10). The internal stress measurements at ULB were performed according to the $d\text{-sin}^2\psi$ method on the (422) peak with 2θ value of 124.7° (CuK α radiation). WTCM/IMO implemented the LIBAD method. The residual stresses observed in the TiN films are large. Type C film exhibit the largest value.

Table 3.2-10: Internal stress obtained by XRD in the TiN coatings.

	a_0	σ WTCM* (GPa)	σ ULB* (GPa)	σ ULB** (GPa)	Measured E (GPa)
TiN-A	4.24334	-9.2	-7.5	-4.6	360
TiN-B	4.24364	-8.8	-5.2	-4.9	320
TiN-C	4.25592	-12	-8.4	-3.9	276

* literature values used for elastic moduli

** measured Young's modulus used + Poisson's ratio = 0.3.

3.2.8.3 XRD stress measurements on Zn

Here, only the $d\text{-sin}^2\psi$ method was used. The coating thickness was large enough to ensure the success of this method. At ULB the (212) peak with 2θ value of 138.9° ($\text{CuK}\alpha$ radiation) was used. The Young's modulus used was 90 kN/mm^2 and the Poisson's ratio 0.3. WTCM used the (112) peak.

Table 3.2-11: internal stress in Zn coatings obtained by the $d\text{-sin}^2\psi$ method.

Sample	Orientation	ULB	WTCM	WTCM
		Isotropical (GPa)	Isotropical (GPa)	Anisotropical (GPa)
Zn-A	Transverse		-0.02	-0.04
	Along	-0.183	-0.08	-0.03
Zn-B	Transverse		-0.01	-0.02
	Along	-0.176	-0.43	-0.17
Zn-C	Transverse		-0.02	-0.01
	Along	-0.183	-0.21	-0.08

3.2.9 Preferential orientation

The TiN-B coating shows a predominantly {111} orientation with a fraction of a {222} orientation. A quasi exclusive (111) orientation is observed for the type A and B films while type C has a quite different structure with a (200) orientation (ULB).

DLC films are amorphous and do not diffract.

Differences can be found in the preferential orientation of Zn. It seems that the Zn-C coating exhibits no specific orientation, the Zn-A a minor orientation and the Zn-B seems to have the strongest orientation. A preferential (101) orientation is observed for the three films. Type C film has a different structure with an (002) orientation (ULB)

3.2.10 DLC structure

Specimens DLC-A and B show Raman spectra typical for diamond-like carbon films: a so-called G-peak at 1540 cm^{-1} and another D-peak at 1350 cm^{-1} (an example is shown in Fig. 3.2-3). The peak positions and widths are indicative of a-C:H type DLC coatings [TAM 94]. The spectrum for coating variant C at the other hand shows only a background signal which is due to the fact that the Raman technique is not sensitive for sp^3 bonded C-H molecules. Therefore, this background pattern is indicative of polymer-like material.

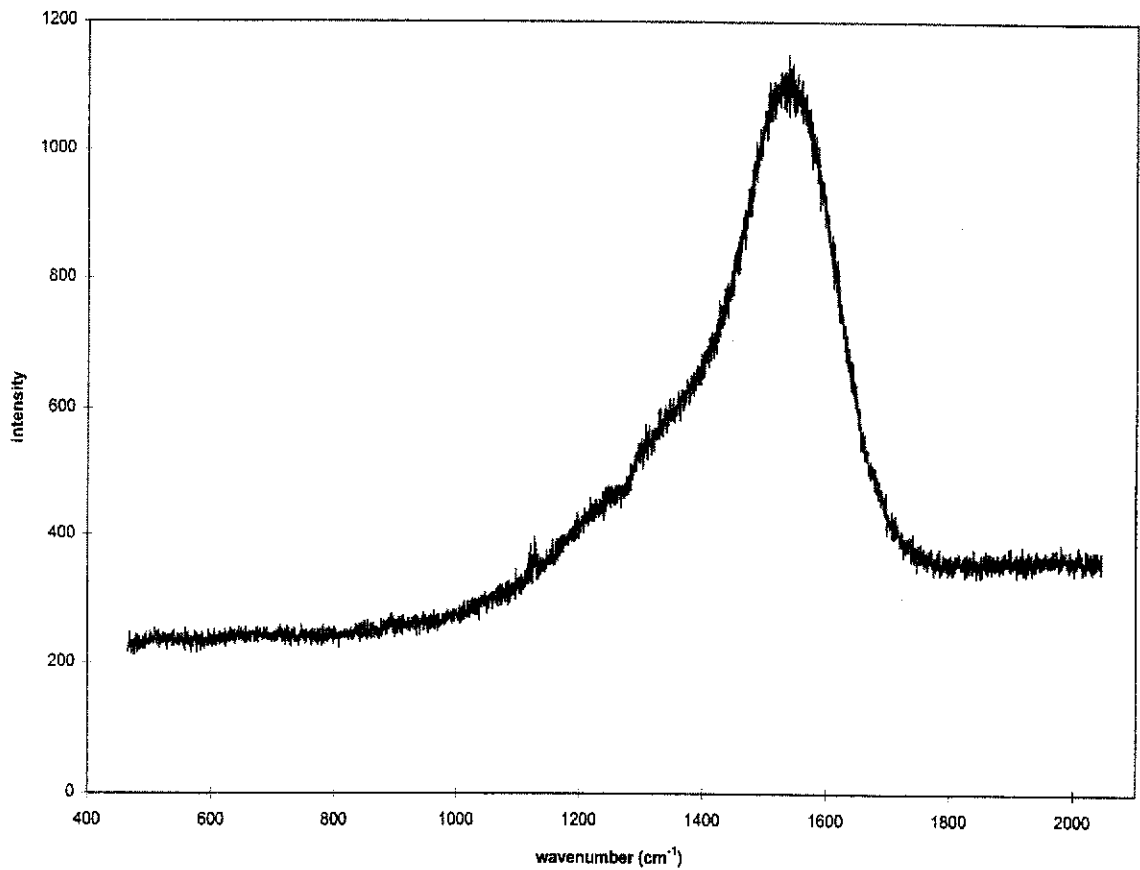


Fig. 3.2-3 Raman spectrum for the coating DLC-A

3.2.11 scratch test

Preliminary scratch testing was done in task B to distinguish between good and poor adhering coatings. By these experiments, it could be verified if the B-type coating really was the less adherent, as was the objective of task A.

The DLC-A and B coatings performed as expected. For the TiN however, the parameters of the deposition had to be adopted during the project. Finally, the Ti interlayer process was modified (no bias) in order to obtain a poor adherent TiN coating, instead of changing the interface layer thickness, which was the original idea. The results are in Fig. 3.2-4.

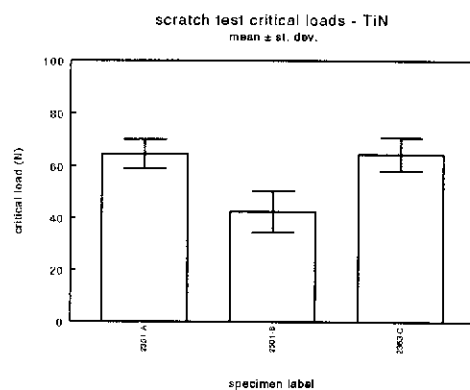


Fig. 3.2-4 preliminary scratch test on the TiN coatings used for task C.

3.3 Adhesion Tests: WP3

3.3.1 scratch tests

3.3.1.1 Single Pass Scratch Test

The average critical load values with standard deviations obtained in the SPST mode are shown in Fig. 3.3-1.

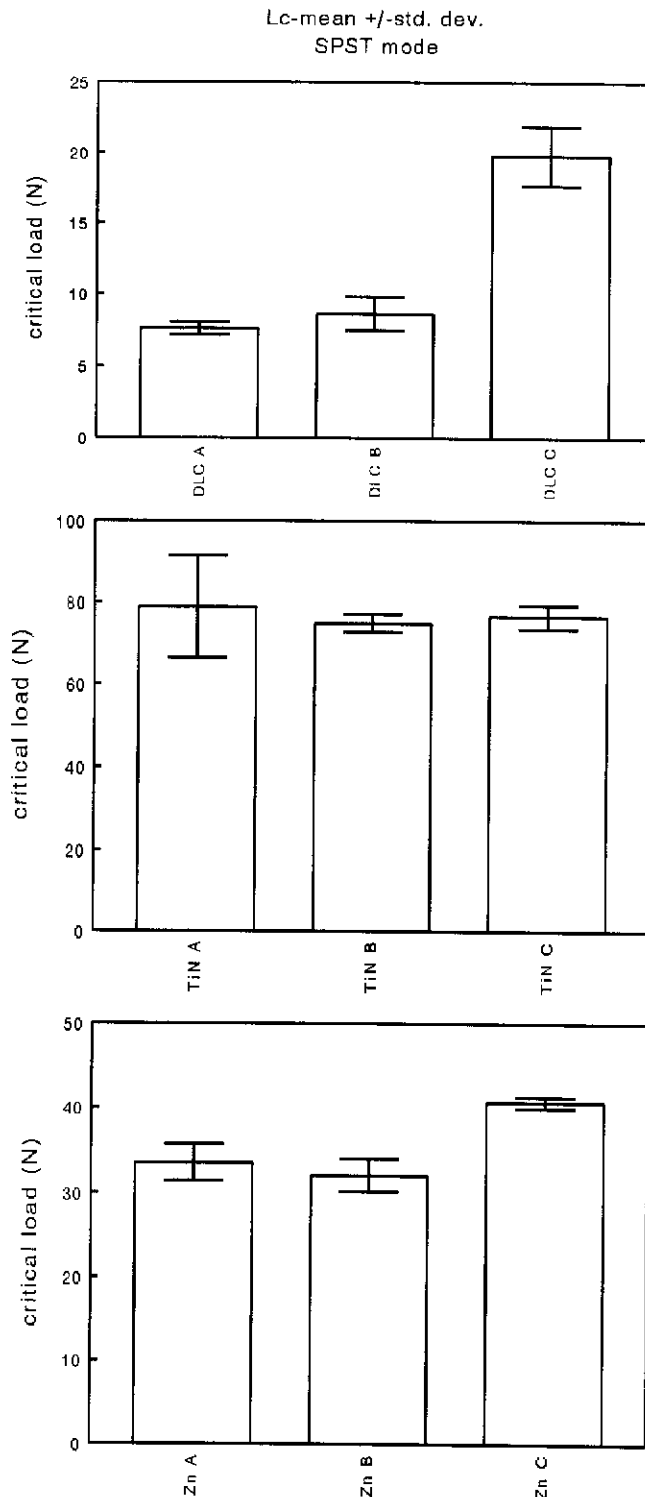


Fig. 3.3-1 Progressive load scratch results of the different types of coatings.

Since the critical load values for the DLC variants A - standard coating with good adhesion, and B - standard coating with poor adhesion, was below 10 N, the loading rate was reduced to 10 N/min. (standard displacement rate of 10 mm/min.), in accordance with pre-Standard ENV 1071-3. For variant C - modified coating structure with good adhesion, standard operating parameters of 100 N/min. and a displacement rate of 10 mm/min. were used. 10 scratches per specimen were carried out.

The average critical load obtained for variant B was slightly higher than for variant A. However, the nature of the failure event was quite different in both cases: while the spallation failures of variant A were restrained to within the scratch track (Fig. 3.3-2a), variant B showed gross flaking in and around the scratch track (Fig. 3.3-2b), which clearly demonstrated the poorer adhesion properties of the latter coating. The scratch direction (SD) is indicated on each picture.

Variant C showed a different failure mechanism and therefore its critical load value cannot be compared to those of variants A and B. The L_c value of variant C was also considerably higher because of the reduced hardness of this coating which allows the spreading of the contact load under the scratch stylus. The higher critical load value obtained for DLC-C thus correlates with its lower internal stresses and hardness value.

EPMA analyses demonstrated that for variants A and B the spallation events occurred at the Si interlayer/substrate interface, while for variant C it occurred at the Si interlayer/top DLC layer interface. SEM micrographs and EPMA chemical mappings are shown in the 2nd 12 month report of Vito.

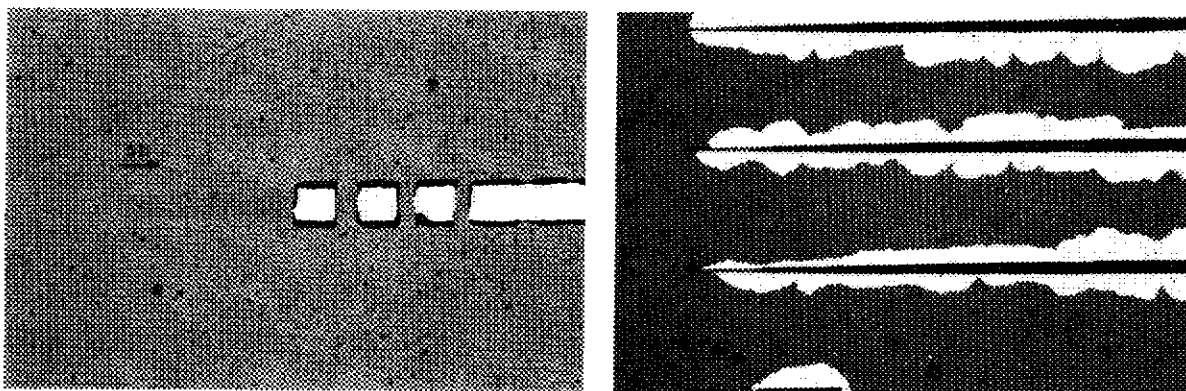


Fig. 3.3-2 failure of the coating at L_c for (a) DLC-A (spallation within the scratch track) and (b) DLC-B (gross flaking in and around the scratch track).

For the TiN variants as well, no significant difference in critical load value for variants A and B could be measured using the progressive load mode scratch test. Moreover, the failure mode and magnitude of the failure events are virtually the same. Both TiN variants spall at the border of the scratch track, exposing the substrate surface (details are given in 2nd 12 month report of Vito). Variant C showed a quite different 'buckling type' failure event and hence its critical load value cannot be directly compared to those of variants A and B (Fig. 3.3-3).

EPMA analyses demonstrated that the spallation events in the case of variants A and B indeed occurred at the Ti interlayer - substrate interface. For variant C, the substrate is much less exposed.

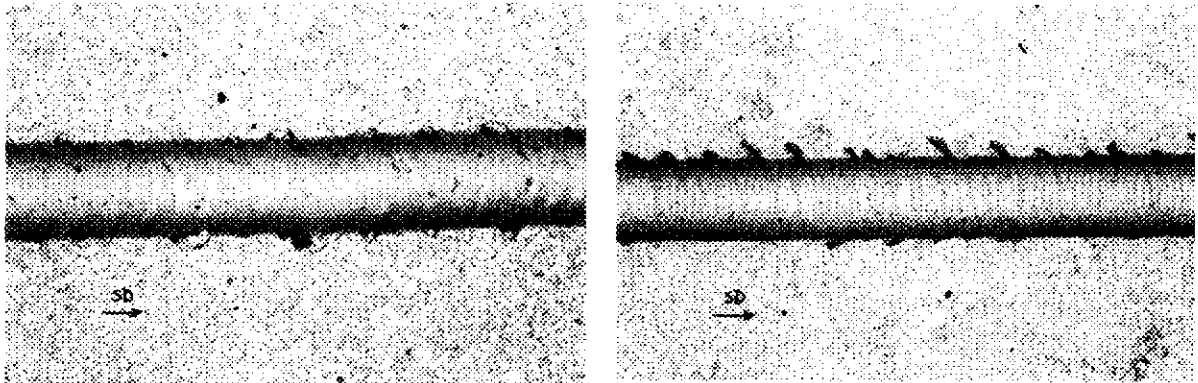


Fig. 3.3-3 failure of the coating at Lc for (a) TiN-A and (b) TiN-C

For both DLC and TiN, the C coating shows a different failure mode, which makes a comparison with the Lc values of the A and B coatings meaningless. Only when the failure mode is similar, a comparison of the Lc values does make sense.

Performing the scratch test on the Zn coatings causes additional problems. Firstly, it was not possible to reveal the iron substrate directly under a reflected light optical microscope due to the absence of colour contrast. An etchant (20 g CrO₃ and 1 g Na₂SO₄ per 100 ml H₂O; 1 - 2 s etch) had to be used subsequent to scratch testing to discriminate between the Zn coating and the Fe substrate. The max. load was set to a sufficiently high value of 100 N.

Secondly, the ductile character of the Zn coatings implies that the stylus simply ploughs through and perforates the Zn coating at a certain normal load, into the iron substrate (see e.g. Fig. 3.3-4). The load at perforation of the coating was assumed to be the 'critical load' in Fig. 3.3-1. The highest critical load value is obtained for variant C, which may be, at least partially, explained simply by the fact that the coating thickness of variant C was higher. However, as the observed failure mode is not related to coating spallation events, it was concluded that the scratch test method cannot be used to characterise the adhesion properties of conventional electro-deposited Zn coatings.

EPMA mappings demonstrated that the used etchant succeeded well in revealing the iron substrate in the scratch track.

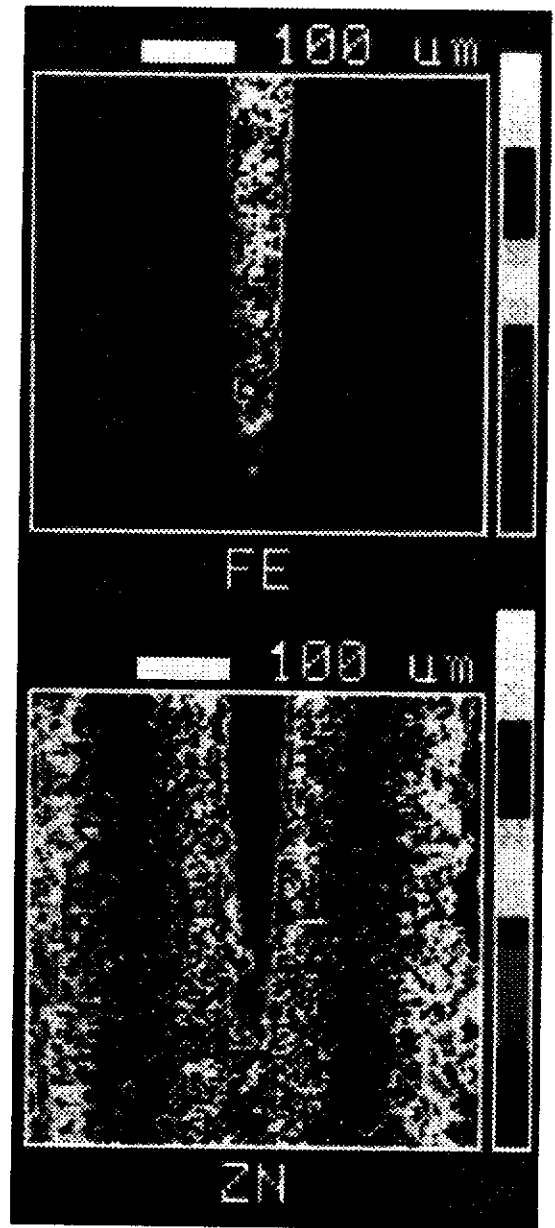


Fig. 3.3-4 Perforation of the Zn coating (optical and EPMA)

behind the scratch stylus. More detailed observation of the track revealed that the coating is wrinkled (= detached but not cracked or spalled) at loads below 7.5 N. These observations are able to explain that for a constant load scratch at 8 N, spallation failure was unlikely to happen for DLC variant A.

The constant load mode scratch test also allowed to demonstrate the poorer adhesion properties of the variant B TiN coating

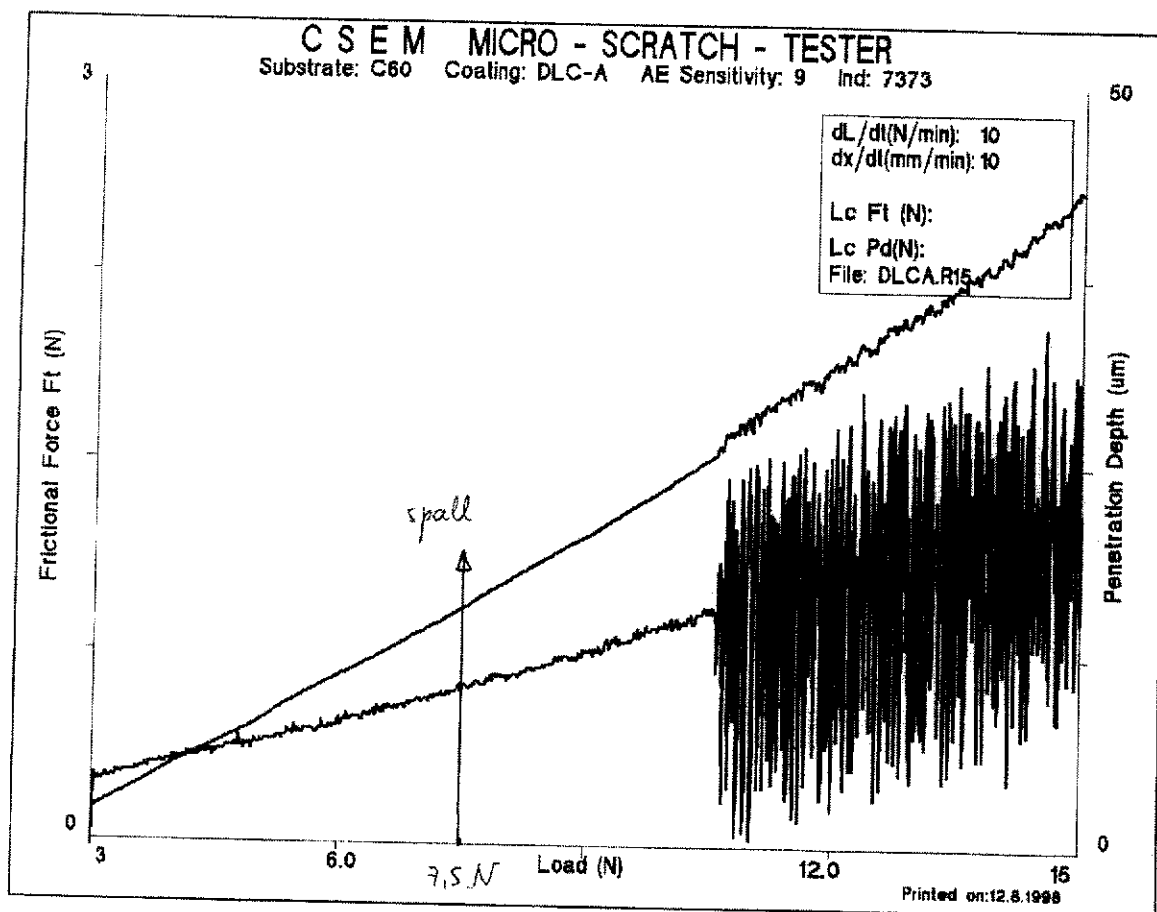


Fig. 3.3-6 Friction force and penetration depth traces for the DLC-A coating, indicating the start of the spallation at a higher load than observed a posteriori in the scratch track.

3.3.1.3 Multipass Scratch Test

The multipass scratch test could not be used to assess the adhesion properties of the three DLC coatings, since no failures were produced even after 25 scratches under 6 N load. This is attributed to the known excellent toughness properties of diamond-like carbon coatings, which prevent the initiation and growth of film cracks that eventually result in coating failure.

Due to the brittle nature of the TiN coatings, repeated scratching in the same scratch track resulted in the progressive damaging of this coating type. The number of scratches used to produce regular spallation failure for the three TiN variants is shown in Fig. 3.3-7. As can be seen, this scratch test mode also enabled to discriminate between the adhesion properties of variants A and B. However, it must be stressed that with the current state-of-the-art equipment, the MPST mode is extremely time- and effort consuming.

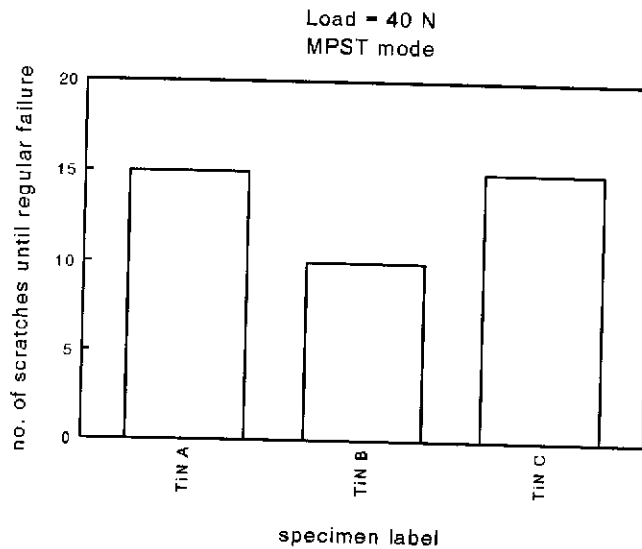


Fig. 3.3-7 Number of MPST passes at 40N to produce regular failure of the TiN variants.

3.3.1.4 Overview

Table 3.3-1: Overview of the scratch test results.

Coating - variant	SPST	CLST	MPST
DLC-A	7.6 ± 0.5	12	not measurable
DLC-B	8.6 ± 1.2	8	not measurable
DLC-C	19.8 ± 2.1	15	not measurable
TiN-A	78.8 ± 12.4	80	15 passes @ 40N
TiN-B	74.7 ± 2.1	60	10 passes @ 40N
TiN-C	76.4 ± 2.9	64	15 passes @ 40N
Zn-A	(33.5 ± 2.2)	(28)	(10 passes @ 15N)
Zn-B	(32.0 ± 1.9)	(28)	(5 passes @ 15 N)
Zn-C	(40.7 ± 0.7)	(40)	(20 passes @ 15N)

The values of the scratch test on the Zn-coatings are indicative. They are not related to the adhesion of the coating.

3.3.1.5 Damage at scratch styli

An interesting additional result is given by the study of the stylus wear during the course of Task C. For each of the three coating types, a different stylus was used: No. 7373 for DLC, No. 7370 for TiN, and No. 7372 for Zn.

From the microscopical observation of the styli (see figures in the 2nd 12 month report of Vito), it is clear that the stylus used to scratch the TiN specimens had suffered severely from wear at its tip. Obviously, this must be due to a combination of the hard TiN surface and the high critical load values, both contributing to high stresses at the stylus tip during operation. Stylus No. 7373 survived the tests on DLC, because of the low frictional properties of this material and the relatively low applied loads.

Obviously, the soft Zn coatings neither produced damage to the diamond stylus.

3.3.1.6 Conclusion

The results of the SPST mode confirm that the critical load value may not be used as stand-alone criterion for the adherence of a coating. Both for DLC and TiN the values of L_c for the good and poor adherent coating are close to each other. However, inspection afterwards show a clear difference in failure event, on which basis a discrimination between good and poor adherence could be made.

When using the scratch test on the Zn coating, a perforation of the coating was obtained without any failure mode related to the adhesion. The stylus is ploughing through the coating material. The scratch test method thus can not be used to characterise the adhesion properties of conventional ductile electro-deposited Zn coatings.

The CLST mode scratch test is more reliable and more sensitive to discriminate coatings on the basis of adherence. Unfortunately, this method is also more time consuming. For the DLC and TiN coatings critical load values were higher for the better adherent types.

The multipass scratch test is even more time- and effort consuming. More information is gained by this test about the toughness and fatigue resistance of the coatings. Due the the excellent toughness properties of the DLC coatings, no coating failure was induced in this mode at a slightly lower load than the L_c obtained by the CLST. The TiN on the other hand showed progressive damaging during the MPST. It was possible to discriminate between the good and poor adherent TiN coatings based on the number of passes before regular spallation failure is observed.

3.3.2 Indentation

3.3.2.1 results

TiN coatings

The indentation tests showed no big difference neither between the different types of TiN coatings nor between the different test conditions although the cracks with the 60 kg load at the A and C coatings were less pronounced. All indentation can be classified in class 1 (VDI-Richtlinie 3198-1991). A representative and typical view is shown in Fig. 3.3-8. The indentations made by the scratch tester at 100 and 200 N did not show any delamination or cracking. A complete overview of the made indentations with the different parameters is given in the 2nd 12 month report of WTCM.

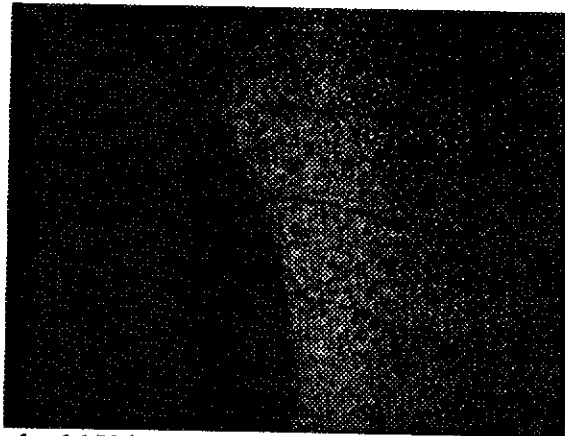


Fig. 3.3-8 TiN-A, load 150 kg, load rate 45[°], hold time 20[°], magnification 256x.

DLC Coatings

Contrary to the TiN coatings the DLC coatings show no cracking, but delamination which is considered a class 6 coating (delamination – bad adhesion), see Fig. 3.3-9. In general, the delamination is bigger when the applied load increases. The load rate nor the hold time seem to affect the test results (delamination throughout). The delaminated zone of the DLC-B coating is larger than of the DLC-A and C.

The indentations made by the scratch tester (low loads) only result in delamination for the DLC-B coating while this effect is not pronounced for the DLC-A coating.

The DLC-C coating on the other hand shows no delamination at high or low loads.. This is probably due to the 'polymeric' nature of this coating. What can be observed is that the coating is 'pushed aside' by the indenter (see also Zn coatings).

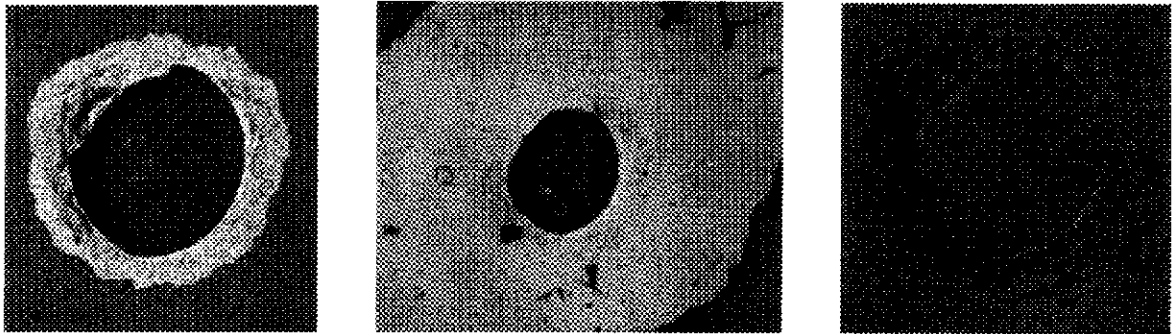


Fig. 3.3-9 From left to right:

DLC-A, load 150 kg, load rate 45", hold time 20", magnification 64x.

DLC-B, load 60 kg, load rate 45", hold time 20", magnification 64x.

DLC-C, load 150 kg, load rate 45", hold time 20", magnification 64x.

Zn Coatings

For the Zn coatings no difference was seen neither between the three coating types of samples nor between the parameters that were to be studied. The coatings are too soft and do not crack while the load is applied. The coating material is pushed aside by the indenter. A typical view is given in .

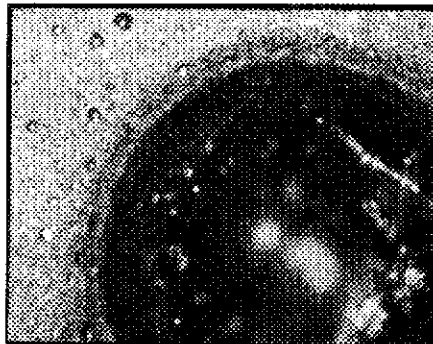


Fig. 3.3-10 Zn-A, load 60 kg, load rate 45", hold time 20", magnification 64x.

3.3.2.2 Conclusion

None of the TiN coatings showed delamination at the used test parameters. The severity of cracking, when it occurred, seemed to be independent of the indentation parameters used in this study (although the 60 kg load produced less cracking for the A and C coatings).

The DLC coatings, except for the C variant, showed delamination independently of the type of coating (good/poor adhesion) nor indentation parameters. The studied A and B DLC coatings fall in class 6 of the above mentioned classification table. The delamination is larger when the applied indentation load is higher. The spallation area is larger for the B than for the A coating at the same load.

The Zn coatings (and the DLC-C coating) showed none of the failures encountered with the other two kind of coatings. Here, the coating is deformed without cracking. A built up edge can be found encompassing the indentation crater.

Based on the above mentioned results and considering the coatings and indentation parameters used in this study the following conclusions concerning the practicability of the indentation test as an instrument to measure the adhesion of coatings could be made:

- the results of the indentation test seem to be independent of the indentation speed and hold time after indentation;
- higher indentation loads cause more delamination for the DLC coatings while a low load (60 kg) gives less pronounced cracking for the TiN coatings;
- the limited number of indentation tests done with the scratch tester (indentation without lateral movement) showed no significant damage for the TiN or Zn coatings but resulted in partial and complete delamination for the DLC-A and DLC-B coatings respectively. This delamination was more severe when a higher load was used (DLC-B); thus enabled to discriminate between the adhesion properties of A and B.
- no spallation events could be provoked in the soft Zn coatings by indentation, hence this method can not be used to assess the adhesion properties of soft coatings.

3.3.3 Four point bending adhesion test

3.3.3.1 results

Table 3.3-2 summarises the results of the 4PB test on the Zn coatings. The type A sample exhibits the highest critical load while the type B sample exhibits the smallest value of critical load. A typical record of the measured load as function of the deflection in the 4PB method is shown in Fig. 3.3-11. The reproducibility of the energy release rate values obtained for type A, B and C coatings is studied. The obtained results are illustrated in Fig. 3.3-12.

Table 3.3-2: Results of the 4PB method on Zn coatings.

	Zn A		Zn B		Zn C	
	P_c (N)	G_c (J/m ²)	P_c (N)	G_c (J/m ²)	P_c (N)	G_c (J/m ²)
specimen 1	1390	292	950	127	1177	208
specimen 2	1360	272	576	61	1124	176
specimen 3	1288	199	811	91	912	116
specimen 4	1187	196	772	75	1061	157
specimen 5	1176	207	626	57	1105	183
		233±45		82±28		168±34

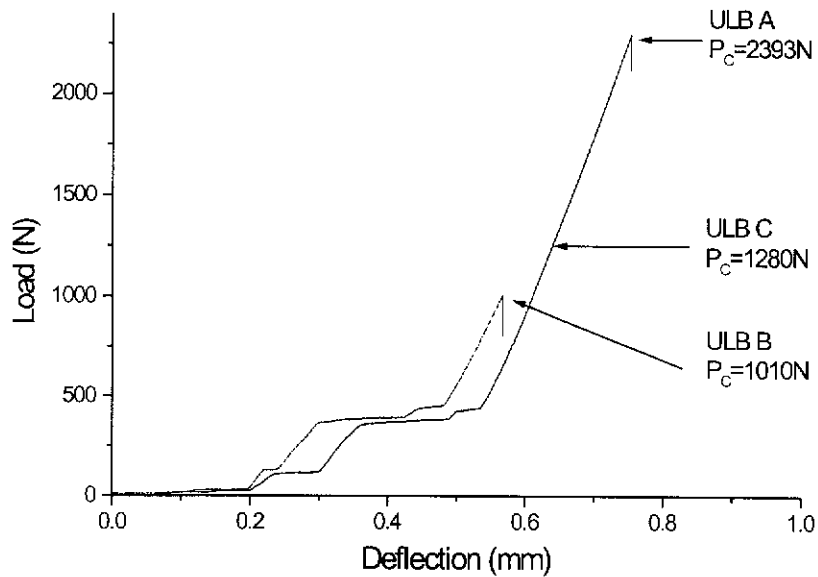


Fig. 3.3-11 Typical output of the 4PB method on Zn coatings.

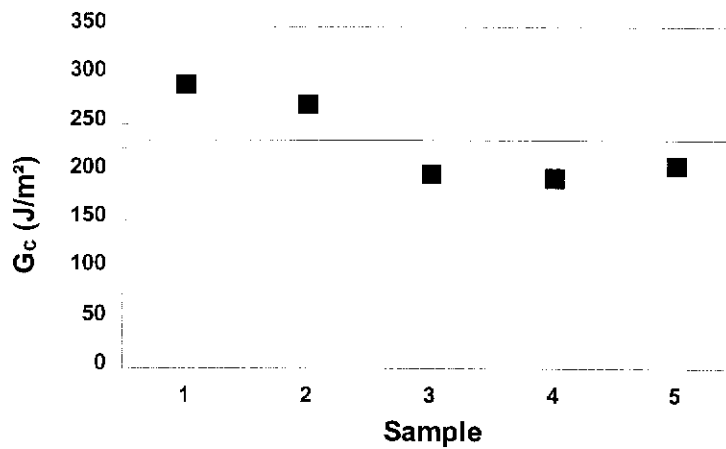


Fig. 3.3-12 Variation of energy release rate for different type Zn-A samples

The first attempts to implement the 4PB testing on the DLC coatings were not successful because the coating flaked off in a region away from the dedicated notch. Finally, a pre-crack could be produced by the selective dissolution of the interface in a concentrated solution of KOH (1 week to produce a crack 2 mm in length). In this way it was indeed possible to use the ‘crack propagation’ method, which yielded a critical energy release rates summarised in Table 3.3-3.

Table 3.3-3: Results of the 4PB method on DLC coatings.

	DLC-A		DLC-B		DLC-C	
	P_c (N)	G_c (J/m ²)	P_c (N)	G_c (J/m ²)	P_c (N)	G_c (J/m ²)
specimen 1	1110	543	295	36	565	100
specimen 2	1200	582	245	19	792	119
specimen 3	1245	609	446	33	758	110
specimen 4	1045	457	174	16	625	104
specimen 5	1217	423	186	14	575	127
		523±80		24±10		112±11

A defect was induced in the TiN coatings by masking during deposition. However, the (glued) interface between upper holder and the specimen failed before any crack propagation between the coating and the substrate was induced. No solution was found for an adequate use of this method on TiN coatings.

3.3.3.2 conclusion

For DLC and Zn coatings the four point bending technique is implemented with success. The method gives a direct measure of the strength of the coating-substrate interface. However, the method is complicated and requires careful sample preparation. The method is not suited for TiN coatings due to the impossibility to induce a defect at the TiN-substrate interface.

3.3.4 Tensile Adhesion Testing

3.3.4.1 DLC-coatings

The tensile test was performed in short increments (0.2%) of the strain. After each step, a metallographic inspection of the surface is made by optical microscopy using surface replicas. This procedure allows to determine the deformation at which cracking of the coating begins. From this initiation strain, the film fracture strength can be calculated (see Table 3.3-4). The Young's modulus determined by DSI is used.

Table 3.3-4: Film fracture strength of DLC coatings.

Specimen	Young's modulus (Gpa)	Crack initiation strain (%)	Film fracture strength (GPa)
DLC A	151	2.0	3.0
DLC B	152	2.3	3.5
DLC C	73	1.8	1.3

Further increasing of the strain of the substrate causes more cracking of the coating. However, after a certain strain, a saturation crack density is reached, as illustrated by Fig. 3.3-13. The corresponding micrograph at the saturation crack density is shown in Fig. 3.3-14. It can be seen that the cracks are parallel and no decohesion is present here. The average saturation spacing was found using image analysis technique and was of about 7.4 μm . The maximum crack spacing found in this part is 23 μm .

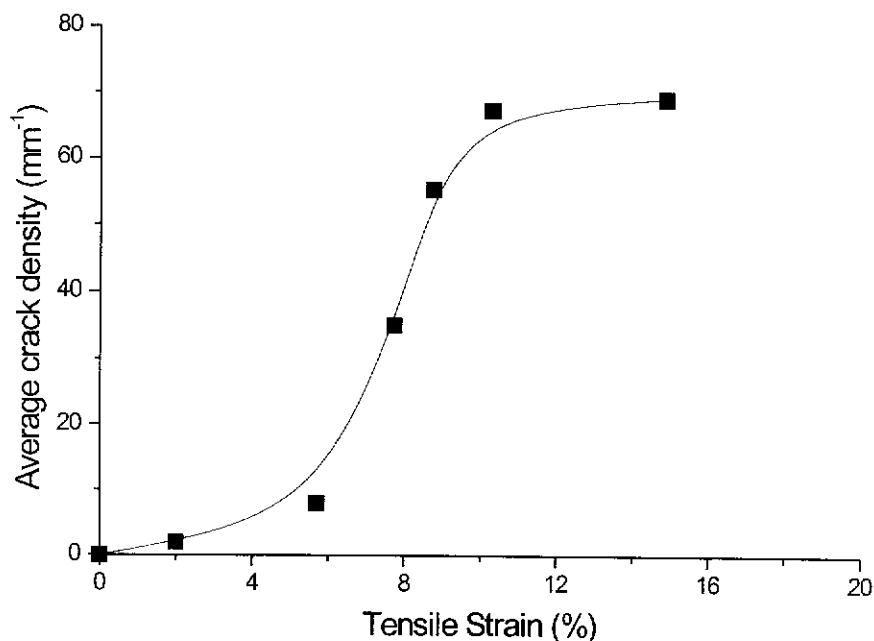


Fig. 3.3-13 Variation of the average crack density with applied strain for the type A DLC film on thin automotive steel.

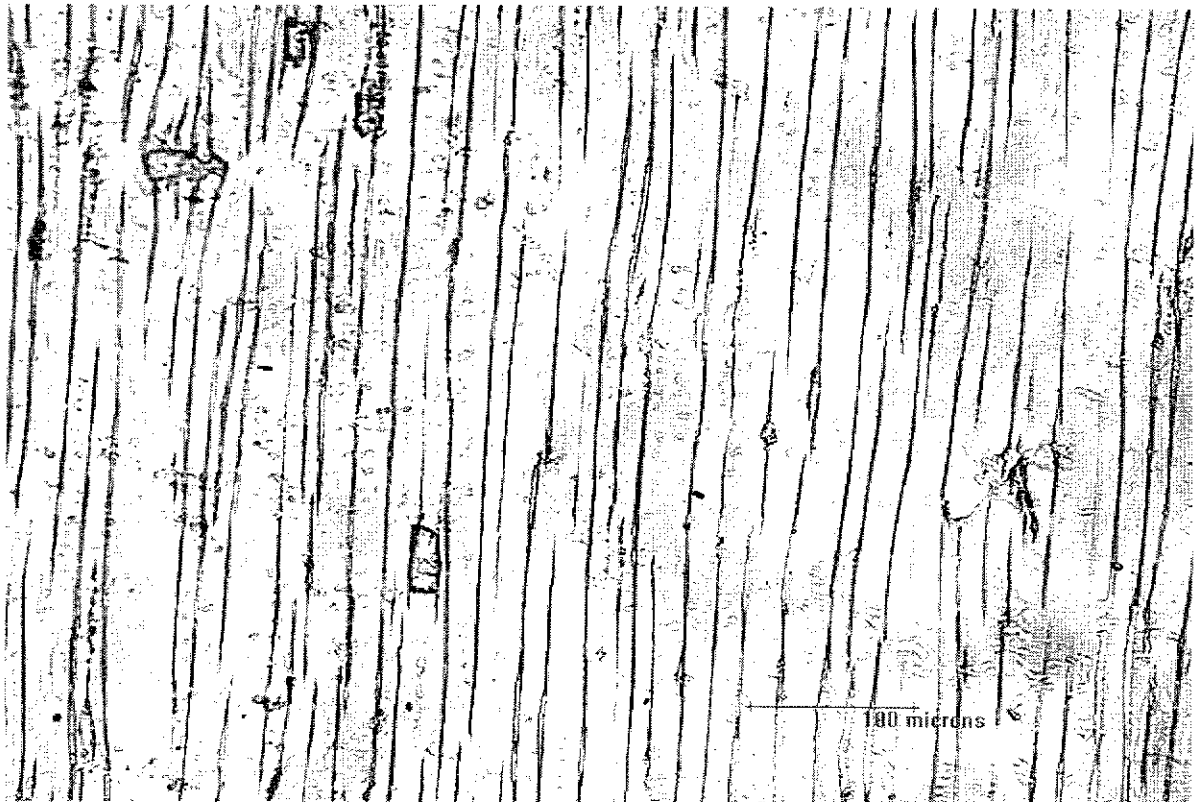


Fig. 3.3-14 Optical micrograph showing the cracks aspect at saturation for type A DLC film on automotive steel.

The distribution of crack spacing at saturation is also of interest. Data for this are presented in Fig. 3.3-15 in the form of cumulative probabilities for crack spacing expressed as film fragment aspect ratio (λ/λ_∞). An approximate indication of the Weibull modulus can be obtained by comparing the experimental spacing distribution with those from the model of Henstenberg and Phoenix. It can be seen that a high value of Weibull modulus ($m \cong 50$) seems to be appropriate for the film. The cracking behaviour of the DLC-A film is quite uniform throughout the film and equation 2.3-10 is applicable without concern in the crack spacing distribution. For the DLC-C coating, the value of m is lower than 50, hence the mechanical properties are more dispersed through the coating.

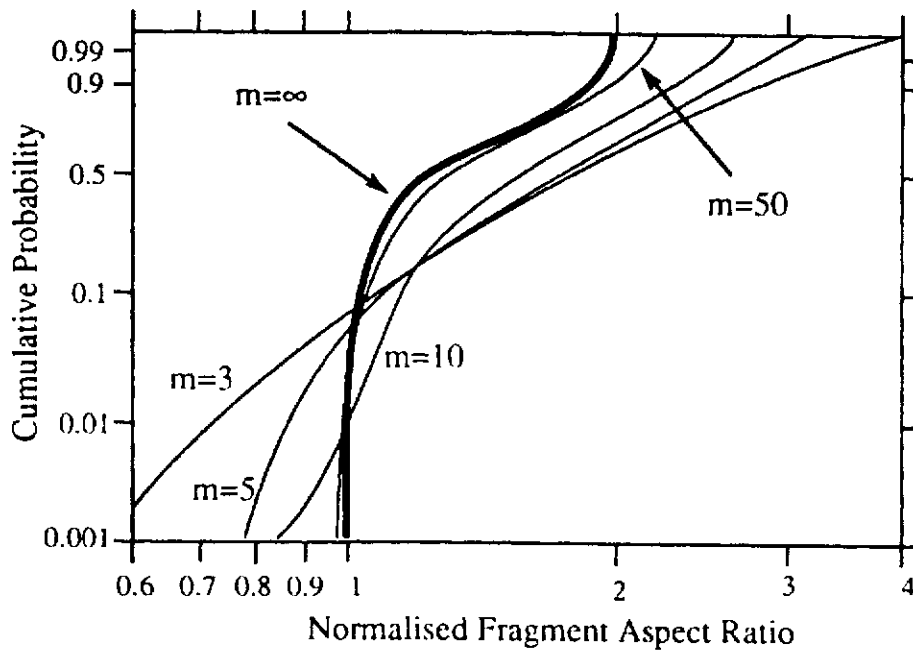


Fig. 3.3-15 Crack spacing distribution data for the type A DLC film on thin automotive steel substrate.

The results by the crack spacing technique are summarised in Table 3.3-5.

Table 3.3-5: Interfacial shear strength calculated for DLC coatings.

Specimen	Average crack spacing (μm)	Maximum crack spacing (μm)	Tyson and Davies	Interfacial shear strength (GPa)			Statistical
				Kelly	Agrawal and Raj	Shieu	
DLC-A	9.38	20.10	2.54 ± 0.59	0.85 ± 0.20	1.33 ± 0.30	1.33 ± 0.30	0.65 ± 0.06
DLC-B	8.98	20.86	2.58 ± 0.48	0.86 ± 0.16	1.35 ± 0.25	1.35 ± 0.25	0.73 ± 0.03
DLC-C	2.26	6.54	1.61 ± 0.32	0.53 ± 0.11	0.84 ± 1.17	0.84 ± 1.17	0.56 ± 0.02

Note that there is a pronounced difference in shear strength between the variants of the DLC-coatings. It is also obvious that the absolute k-value is strongly dependent on the model one adopts.

Although the values of the DLC-A and DLC-B are close together, a complete different phenomenon is observed on the DLC-B coating. Indeed, there was severe spallation of the DLC-B coating while performing the tensile test. The models as used above are no longer valid in that case. Instead, the steady state delamination strain ϵ_d° and the lower limit of the debonding energy γ can be calculated. The results are given in Table 3.3-6 together with the values of the fraction A (%) of the delaminated area.

Table 3.3-6: delamination strain, bonding energy and spalled surface fraction for DLC-B. The average over 5 different specimen is given.

Specimen	ϵ_d° (%)	γ (J/m^2)	A (%)
DLC-B	3.0 ± 0.3	195 ± 41	19.6 ± 2.1

The values of γ are much higher than those found in § 3.3.1, probably due to the internal stress present in the coating and not taken into account in the calculation.

3.3.4.2 TiN coatings

The same procedure has been followed as for the DLC coatings. The results are summarised in Table 3.3-7 and Table 3.3-8. The details are given in the 18 month progress report of ULB. No spallation is observed for the TiN coatings.

Table 3.3-7: Film fracture strength of TiN coatings.

Specimen	Young's modulus (Gpa)	Crack initiation strain (%)	Film fracture strength (GPa)
TiN A	360	3.1	3
TiN B	320	2.6	3.4
TiN C	276	2.2	2.2

Table 3.3-8: Interfacial shear strength calculated for TiN coatings.

Specimen	Average crack spacing (μm)	Maximum crack spacing (μm)	Tyson and Davies	Interfacial shear strength (GPa)			Statistical
				Kelly	Agrawal and Raj	Shieu	
TiN-A	5.82	16.50	4.27 ± 0.60	1.42 ± 0.20	2.23 ± 0.31	2.23 ± 0.31	1.48 ± 0.04
TiN-B	5.24	17.76	4.71 ± 1.56	1.57 ± 0.52	2.46 ± 0.81	2.46 ± 0.81	1.85 ± 0.11
TiN-C	7.96	25.56	1.64 ± 0.18	0.55 ± 0.06	0.86 ± 0.10	0.86 ± 0.10	0.65 ± 0.03

3.3.4.3 Conclusion

Characterisation of strength and adhesion of brittle film on ductile substrate is possible using a simple tensile test.

Different models exist to obtain the maximum interfacial shear strength from the film thickness, the tensile fracture strength of the film and the maximum crack spacing. Crack spacing distribution provides information about the film strength distribution. If the crack spacing distribution is scattered, the utilisation of the average value of the spacing to evaluate the interface shear strength is more appropriate.

In some systems, film cracking may be accompanied by interface decohesion. If steady state condition develop, the energy release rate for films decohesion may be evaluated.

The relative values of τ_I obtained in the tests at ULB are subject to numerous remarks:

- The value of the DLC-B coating cannot be used because there is delamination of the coating. Part of the coating had flaked off from the substrate. The models, however, assume that the cracked coating segments remain bonded to the substrate. Scanning acoustic microscopy could be used to verify such behaviour.
- If the measured (macro-)stress in the DLC coatings is taken into account, the absolute value of DLC-A and DLC-C are closer to each other.
- In the case of TiN, the internal stress (IS) measured by XRD is taken into account. However, the situation here is much more complicated. Internal stresses measured by XRD correspond to the local stress, i.e. the sum of the macrostress and micro- or intrinsic stress is obtained. When the coatings cracks, only the macrostress is relaxed. In this work, no distinction was made between micro- and macrostress.
- Finally, the method is obviously not suitable for ductile coatings.

3.4 Overview of the Results

Technique	Scratch Test SPST	Scratch Test CLST	Scratch Test MPST	Indentation Test	Crack Propagation Test	Crack Spacing Test
Measure	Lc [N]	Lc [N]	number of passes	class	Gc [J/m ²]	τI [Gpa]
DLC A	7.6	12	-	6	523	1.33
DLC B	8.6	8	-	6	24	(1.35)
DLC C	19.8	15	-	no failure	112	0.84
TiN A	78.8	80	15 passes	1	-	2.23
TiN B	74.4	60	10 passes	1	-	2.46
TiN C	76.4	64	15 passes	1	-	0.86
Zn A	-	-	-	-	233	-
Zn B	-	-	-	-	82	-
Zn C	-	-	-	-	168	-

4 CONCLUSIONS

4.1 General Conclusions

- Scratch test
Inspection of the scratch track is a necessary to determine critical load values.
CLST and MPST are better than SPST to assess adhesion properties of coatings, but these procedures are currently too effort-consuming.
The test cannot be used for ductile coatings (Zn).
- Indentation Test
Same conclusion as for the scratch test.
In general, less information is obtained, although subsequent indents at increasing normal loads would be a valuable alternative for the scratch test.
- Crack propagation technique
The test is only applicable if a precrack at the interface can be generated in situ, during the coating process.
For the Zn coatings, the results are as expected. The same is true for DLC, except for type C, due to a different failure mechanism.
- Crack spacing technique
The test cannot be used for ductile coatings (Zn).
For DLC, the results are as expected, except for type B, where spallation occurred. As a matter of course, in the latter case the poor adhesion is qualitatively demonstrated.
For crystalline materials, the analysis may be more complicated than the currently proposed models, in particular for highly stressed coatings.

4.2 Future research issues

Although the scratch test is a valuable engineering test for the evaluation of coating adherence, it still can be refined. The scratch test Atlas of failure modes needs to be refined and extended. For the scientifically sound classification of failure events, a good understanding of the mechanisms of failure is indispensable. In a current SMT project, "Multimode Scratch Testing" – MMST (SMT4/97-2150), in situ video monitoring and enhanced signal capturing and processing techniques are being developed, which will greatly facilitate the understanding of scratch test failure mechanisms.

Only some of the observed failure events in scratch testing are related to detachment at the coating/substrate interface and are thus relevant as a measure of adhesion. Other failures, such as cracks and cohesive damage within the coating or substrate may be equally important to determine the behaviour of a coated component in a particular application. The scratch test should indeed be regarded as a repeatable tribological test to assess the mechanical integrity of a surface, including bulk materials. Within this scope, it would be a big step forward if the operation modes were to be extended, to include for example constant load (uni-axial and reciprocal) test procedures. The latter is one of the targets of the aforementioned MMST project.

Another important issue would be the extension to smaller scale (micro-, nano-) contacts to enable the probing of near surface (coating-only) properties, much alike the evolution from the conventional hardness tests to the current nano-indentation technique. This would require, inter alia, the use of sharper styli and higher load resolutions and hence, enhance calibration procedures and measurement skills.

The indentation adhesion test will also be incorporated in the aforementioned MMST project.

Finally, it is evident that the crack spacing technique is the less mature. Thorough scientific understanding of the influencing parameters on the crack nucleation and growth is a necessary. Unfortunately, investigations done in that field are still scarce. Further normative research is needed to establish the sensitivity of the method to different test parameters, to track the reproducibility and to quantify the error budget of the technique.

References

- [ACK 94] K. Van Acker, L. De Buyser, J.P. Celis, P. Van Houtte, *J. Appl. Cryst.* **27**, 1994, 56
- [AGR 89] D.C. Agrawal and R. Raj, *Acta metall.* **37**, 1265 (1989).
- [BEN 89] J.M. Bennett and L. Mattsson, Introduction to Surface Roughness and Scattering, Optical Society of America, Washington, D.C., 1989
- [BOW 73] O.L. Bowie, *Methods of Analysis And Solutions of Crack Problems* (edited by G.C. Sih). Noordhoff, Holland (1973).
- [CHI 92] C-C. Chiu, *Mater. Sci. Eng.*, A150 (1992) 139
- [DEK] E. Dekempeneer, J. Smeets, J. Meneve, Method for applying a diamond-like carbon coating on steel, iron and alloys thereof, EP 0 600 533 B1
- [FRE 68] A.M. Freudenthal, in H. Liebowitz (ed.), *Statistical Approach to Brittle Fracture*, vol 2, *Fracture*, Academic Press, New York, 1968, Chap 6.
- [GIL 83] G.Gille, *Thin Solid Films* **110**, 37-54 (1983).
- [GIL 84] G.Gille, *Thin Solid Films* **111**, 201-218 (1984).
- [HEN 89] R.B. Hentsenberg and S.L. Phoenix, *Polymer Comp.* **10**, 389 (1989).
- [HU 89] M.S. Hu and A.G. Evans, *Acta metall.* **37**, 917-925 (1989).
- [KEL 66] A. Kelly, *Strong Solids*, Clarendon Press, Oxford (1966).
- [OLI 92] W.C. Oliver and G.M. Pharr, *J. Mater. Res.*, 7 (1992) 1564
- [RAM 91] P.M. Ramsey, H.W. Chandler and T.F. Page, *Thin Solid Films* **201**, 81-89 (1991).
- [SHI 90] F.S. Shieu, R. Raj and S.L. Sass, *Acta metall.* **38**, 2215 (1990).
- [SUO 89] Z. Suo, *Mechanics of Interface Fracture*, U.M.I. Dissertation Information Services (1989).
- [TAM 94] M.A. Tamor et al.,
J. Appl. Phys., 76 (6) (1994) 3826
- [TYS 65] W.R. Tyson and G.J. Davies, *Br. J. appl. Phys.* **16**, 199 (1965).
- [VOR 93] M.A. Voronkin, S.N. Dub, I.N. Lupich and B.A. Maslyuk, *Diamond and Related Materials* **3**, 116-118 (1993).

Referred standards

ASTM Standard E 178-80

pre-Standard ENV 1071-3:1994 'Determination of Adhesion by the Scratch Test'

ISO 3290

EN 10109-1:1995

VDI-Richtlinie 3198-1991

Publications

M. Ye, G. Berton, J.-L. Delplancke, M.-P. Delplancke, L. Segers, R. Winand and K. De Bruyn, 'Residual stress evolution by ex-situ annealing of TiN thin films deposited on steel substrates', *Materials Science Forum*, Vols. 287-288, (1998), 275-280

M. Ye, J.-L. Delplancke, G. Berton, L. Segers and R. Winand, 'Characterization and adhesion strength study of Zn coatings electrodeposited on steel substrates', *Surface and Coatings Technology*, 105, (1998), 184-188

J. Meneve, K. Vercammen, E. Dekempeneer, J. Smeets, 'Thin tribological coatings: magic or design?', *Surface and Coatings Technology*, 94-95 (1997) 476.

J. Meneve, P. Andersson, D. Camino, N.M. Jennett and J. von Stebut, 'The scratch test: a sensitivity and reproducibility study', *Abstracts of papers from the World Tribology Congress, London, 8-12 September, 1997*, p. 60 (extended abstract).

J. Meneve, J. von Stebut, N.M. Jennett, D. Camino, P. Andersson, 'The scratch test: Atlas of failure modes', *Abstracts of papers from the World Tribology Congress, London, 8-12 September, 1997*, p. 495 (extended abstract).

E. Matthaei-Schultz, H. Vettters, J. Meneve, N. Jennett, M. Gee, T. Randles, L. Robert, J. von Stebut, 'Hard coatings forced to prove their mettle', *Vacuum Solution*, August/September 1998, 29.

Distribution List

F. Monteny - OSTC (2 copies)
D. Neerinck - Bekaert CRC
F. Van Dooren - Cockerill CRD
A. Piccinin - Union Minière R&D
R. Dekeyser - Agfa Gevaert
H. Vettters - IWT Bremen
S.R.J. Saunders - NPL CMMT
L. Segers - ULB
K. De Bruyn – WTCM
J. Meneve – Vito
K. Van Acker - Vito
Vito - Bib
Vito - SEKMAT
CEN TC184 WG5 study group